Spotlight: Visualization of Moiré Quantum Phenomena in Transition Metal Dichalcogenide with Scanning Tunneling Microscopy

Hao Zhou[a,b*], Kangkai Liang[a,b*], Liya Bi, Yueqing Shi[a, b], Shaowei Li[a,b +]

[a] Department of Chemistry and Biochemistry, University of California, San Diego, La Jolla, CA 92093-0309, USA

[b] Materials Science and Engineering Program, University of California, San Diego, La Jolla, CA 92093-0418, USA

Abstract:

Transition metal dichalcogenide (TMD) moiré superlattices have emerged as a significant area of study in condensed matter physics. Thanks to their superior optical properties, tunable electronic band structure, strong Coulomb interactions, and quenched electron kinetic energy, they offer exciting new avenues to explore correlated quantum phenomena, topological properties, and light-matter interactions. In recent years, scanning tunneling microscopy (STM) has made significant impacts on the study of these fields, by enabling intrinsic surface visualization and spectroscopic measurements with unprecedented atomic scale detail. Here, we spotlight the key findings and innovative developments in imaging and characterization of TMD heterostructures via STM, from its initial implementation on the in situ grown sample to the latest photocurrent tunneling microscopy. The evolution in sample design, progressing from a conductive to an insulating substrate, has not only expanded our control over TMD moiré superlattices but also promoted an understanding of their structures and strongly correlated properties, such as the structural reconstruction and formation of generalized two-dimensional Wigner crystal states. In addition to highlighting recent advancements, we outline upcoming challenges, suggest future research direction, and advocate for the versatile use of STM to further comprehend and manipulate the quantum dynamics in TMD moiré superlattices.

Keywords: moiré superlattice; transition metal dichalcogenide; scanning tunneling microscopy, quantum phases.

* These two authors contribute equally.

+ Correspondence should be addressed to shaoweili@ucsd.edu

1. Introduction

Transition metal dichalcogenides (TMDs) have emerged as a promising and dynamic area of research within condensed matter physics, primarily due to their two-dimensional nature in combination with remarkable magnetic[1-13], optical[14-30], and electronic[31-49] properties that hold the potential to revolutionize various technological applications and fundamentally enhance our understanding of the material. TMDs are characterized by the general formula MX_2 where M represents a transition metal and X denotes chalcogen. The weak interlayer van der Waals interaction allows the easy preparation of monolayer TMDs by mechanical exfoliation[50-53], as well as the fabrication of heterogeneous junctions by superposing TMD layers on top of each other[54-58]. By controlling the applied material, stacking order, or twist angle, the properties of the heterostructure can be engineered with unprecedented tunability[59-70]. Specifically, moiré superlattice can form when the structures of adjacent layers are close to commensurate, creating a long period periodicity due to the small lattice mismatch[71, 72]. This could be formed either by twisting layers of the same material at an appropriate angle, or by aligning two different materials with a small lattice difference. In the momentum space, the superlattice defines another Brillouin zone with a smaller reciprocal lattice, which folds the parabolic band structure defined by the atomic lattice into a sequence of new bands characterized by remarkably narrow bandwidths, commonly referred to as moiré flat bands[73-83]. Similar to their graphene counterparts, these TMD moiré superlattices have undergone extensive investigation in both theoretical studies and experiments, primarily because of the diverse quantum phenomena they facilitate.

While graphene has garnered significant attention as a two-dimensional material for its high accessibility[84-94], high symmetricity[95-106], and superior carrier mobility[107-118], TMD moiré systems offer unique advantages. Firstly, compared to graphene, which consists solely of carbon atoms, TMDs provide a versatile range of materials achieved by substituting either the transition metal or the chalcogen atoms within the same group. Numerous TMDs, such as MoS_2 and WSe_2, share similar atomic structures but possess distinctive electronic properties[35, 119-122]. This abundance of options in building blocks offers a multitude of choices for crafting functional devices tailored to specific applications[2, 25, 27, 35, 38, 40, 41, 123-127]. Secondly, the natural existence of a bandgap close to the visible range in most TMDs also makes them suitable for a

broad range of optoelectronic applications[15, 16, 128-131]. Moreover, the incorporation of heavy transition metals into the structural framework significantly enhances spin-orbit coupling, holding promise for various spintronic applications[132-145]. Most strikingly, the reduced dimension, together with limited dielectric screening from the surrounding, leads to a substantial amplification of the Coulomb interaction[81, 146-153]. Likewise, the creation of ultra-narrow moiré flat bands can effectively modulate the charge carrier behaviors in them. The kinetic energy of the electrons residing in these flat bands becomes significantly restricted[81, 154-157]. Consequently, the Coulomb interaction frequently takes precedence in electron interactions, leading to the emergence of a sequence of highly correlated quantum phenomena including tightly bonded moiré exciton[149, 158-168], correlated insulator[148, 150, 152, 169-177], and charge order states[146, 148, 149, 151, 178-185]. Unlike the magic angle sensitivity of graphene, TMD moiré systems exhibit these strongly correlated properties in much less stringent conditions[81, 82, 186-189]. While the moiré flat bands in TMDs may possess less topological character[153, 190-198] compared to those in graphene, they offer a dedicated platform for investigating strongly correlated phenomena.

These strongly correlated systems often involve periodic alternation in a small spatial region or undergo phase transitions in response to nanoscale environments where their properties change significantly, high spatial resolution enables the mapping of the spatial distribution of different quantum phases, helping to identify critical points and boundary regions that might not be apparent at larger scales. To enable the atomic-scale visualization of surface topography and spectroscopic measurements, scanning tunneling microscopy (STM), together with a few other real space imaging approaches[172, 199-214], has been introduced to study TMD moiré systems. The unparalleled spatial resolution of STM, derived from the exponential relationship between quantum tunneling probability and the distance between the tip and a substrate, significantly empowers the direct imaging of the moiré pattern and the identification of its periodicity and phase[215, 216]. Scanning tunneling spectroscopy (STS) further helps to provide detailed information about the local electronic structure, allowing for the identification of flat bands and other unique electronic features. For TMD moiré superlattices on conductive substrates, STM has been instrumental in validating the formation of an unexpectedly large periodic potential[217], which facilitates the formation of flat bands. For TMD moiré superlattices on insulating substrates, STM, by circumventing phenomena such as Fermi level pinning and

electronic screening[218-220], has provided a more intrinsic view of the moiré flat bands, the sensing and manipulation electron-electron correlation, the direct observation of the 2D generalized Wigner crystal lattice in real space, and the visualization of photoexcited moiré excitons. This spotlight article explores the pivotal role of STM in elucidating the structural and electronic properties of TMD moiré superlattices, tracing the progress of the exploration of the strongly correlated quantum phenomena hosted by these systems.

2. Recent STM Studies on TMD Moiré Heterostructures

2.1 STM Studies on TMD Moiré Heterostructures on Conductive Substrates

To understand the stacking configurations and interlayer coupling in moiré superlattice, in 2017, Chendong et al. employed STM to image the R stacking (zero-degree rotational angle) MoS_2/WSe_2 hetero-bilayers grown on graphite surface under various bias voltages[221]. Their work utilized scanning transmitted electron microscope (STEM) to resolve the stacking types [AA AB_{Se} Bridge (Br) and AB_w] within a superlattice [Fig. 1(A)&(B)], complemented by first-principles calculations to predict critical points in the electronic structure, such as K_w, Γ_w states. These critical points expected a direct gap could be maintained in the bilayer and were then measured using STS [Fig. 1(C)]. Based on the Tersoff-Hamann model, the dI/dV signal measured in STS is directly proportional to the local density of states (LDOS). In this study, the authors also utilized a less common approach, by keeping the feedback loop close and measuring the differential change of tip height at different bias voltage $(\partial Z/\partial V)_I$ [Fig. 1(D)]. Different to the traditional dI/dV, the $(\partial Z/\partial V)_I$ measurement provides additional sensitivity to the states that decay fast in the z-direction. By comparing the dI/dV spectra and the valence bands' $(\partial Z/\partial V)_I$ and decay constant k spectra [Fig. 1(E)] for different local alignments, they observed a sudden drop in the $(\partial Z/\partial V)_I$ spectrum, when the sample bias shifted from below to above Γ_w states in the WSe_2 layer. This confirmed the loss of Γ_w states, which arises from different lateral alignments of the S/Se' p_z orbitals at various tacking types. This result was further proved by the local minimum behavior in the k spectrum for the parallel momentum $k_{||}=0$ at Γ point and $k=\sqrt{\frac{2m\phi_0}{\hbar^2}+k_{||}^2}$, where ϕ_0 is the barrier height. After cohesively analyzing the behaviors on both VBM and CBM on different sites [Fig. 1(F)], they found that the local bandgap E_g is site-dependent, resulting in a periodic modulation as large as 0.2 eV, hence an

electronic superlattice [Fig. 1(G)&(H)]. This has been further validated by bias-dependent STM images wherein states at different sites gradually moved out of the tunneling window.

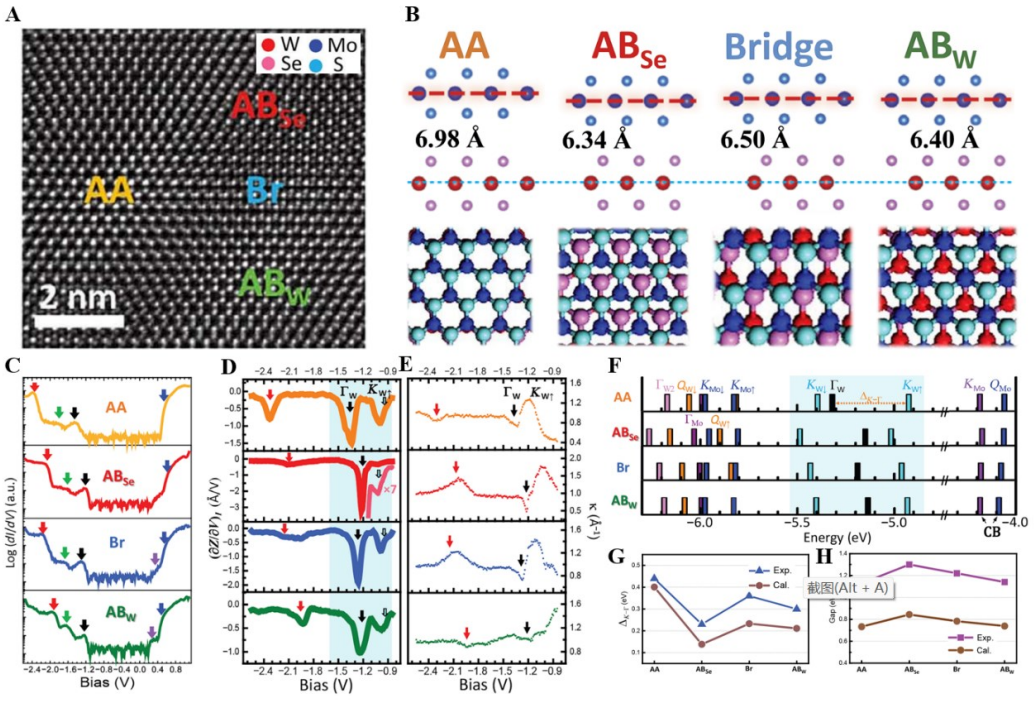

Fig. 1 (A) Atomically resolved STEM image. Typical regions in an R-stacked heterostructure—AA, AB_{Se}, Br, and AB_W—are labeled. The top views and side views of simulated atomic models (based on an R-type stacking) are displayed in (B) respectively. The calculated interlayer separations for four atomic alignments are labeled in (B). dI/dV spectra (C), $(\partial Z/\partial V)_I$ (D), decay constant k spectra of valence bands (E), and calculated energy values at key critical points (F) for AA, AB_{Se}, Br, and AB_W sites are displayed respectively. The energies are with respect to the vacuum level. The shaded regions in (D) and (F) represent the valence band edges and show consistent movements of the energy locations of Γ_W (black) and K_W (cyan). In a deeper lying energy range, the spectral features marked by red and green arrows in (C) to (E) correspond to the energy window where the lower energy states labeled in (F) are located. The complicated movements in their relative energy locations result in a complex behavior in k spectra [red arrows in (E)]. (G) Energy differences between K_W and Γ_W ($\Delta_{K-\Gamma}$) for the four atomic alignments via experiments and DFT calculations. (H) Local bandgap E_g formed between the CBM of MoS_2 and the VBM of WSe_2 via experiments and DFT calculations.

the moiré corrugation remain, unreported sharp peaks appear in the tunneling spectra near the band edge for Γ_W VB at AB_W and AB_{Se} and for K_M CB at AB_W and disappear at higher temperature (80 K) [Fig. 2(A)&(B)]. These peaks were attributed to quantum-confined states in the moiré unit cell, which were further demonstrated by the distinct rings around AB_W in the constant-height conductance map at +0.6V [Fig. 2(C)&(D)]. The spatial conductance maps along the line for CB and VB are also consistent with the previous statement, where two AB_W-

confined states are observed in the CB region and confined states at AB_W and AB_{Se} are observed in the VB region [Fig. 2(E-H)]. To explain the origin of these spectral peaks, Yi et al. employed a nearly free electron (NFE) model on a hexagonal moiré lattice with the potential term $|V_G|$=21meV and derived the wavefunction at the Γ_w point, which shows strong confinement of the state at AB_{Se}. However, it is important to note that the MoS_2/WSe_2 heterostructures used in both studies were grown using chemical vapor deposition (CVD), which can present limitations in terms of sample quality, as well as control over the stacking order and twist angle. Besides, the conductive substrate could largely screen the Coulomb interaction, potentially hindering the formation of strongly correlated phases[218-220].

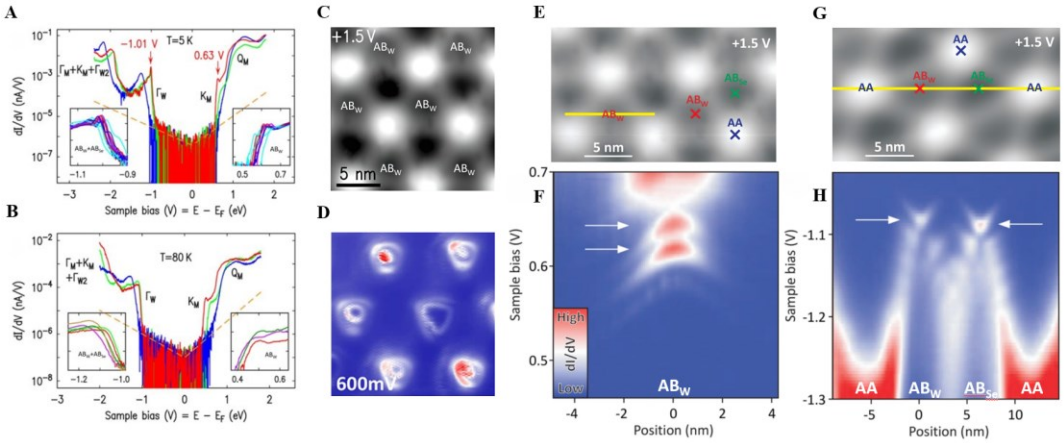

Fig. 2 Selected STS data acquired at 5K (A) and at 80K (B) for different local alignments, with insets showing expanded view of band-edge peaks and including data from nearby spatial locations. Here the blue, red, and green lines correspond to AA, AB_W, and AB_{Se} site respectively. (C) A STM constant-current image of heterobilayer of MoS_2 on WSe_2. (D) A constant-height conductance map acquired at 600 mV. In (D), distinct rings are seen around AB_W, which are associated with quantum-confined states in the moiré unit cell. (E) STM image, with moiré locations AA, AB_W, and AB_{Se} indicated. (F) Constant-height conductance map taken along the yellow line in (E) for voltages in the conduction band-edge region, revealing two AB_W-confined states (marked by arrows) and the band onset at higher energy (broader AB_W-centered conductance feature). (G) Same as (E) but at a different area of the MoS_2–WSe_2 moiré structure. (H) Constant-height conductance map taken along the yellow line in (G) for voltages in the valence band-edge region; confined states occur at locations AB_W and AB_{Se}. All measurements from (C) to (H) are operated at 5K.

symmetry[223]. The superlattice was transferred onto a graphite substrate and then measured with STM and STS [Fig. 3(A)]. While the 0° (AA) rotation breaks the inversion symmetry in TMD, the 60° (AB) rotational symmetry maintains, which is different with the twisted bilayer graphene systems. The authors directly measured moiré flat bands and localized states using

STS and observed distinct differences between these two angles. In the case of 3° twisted bilayer WSe_2, the flat band was found to be localized on the hexagonal network between the AA sites, while the first flat band in 57.5° twisted layer WSe_2 was localized on the AB sites. Constant-height STS measurements of 3° twisted bilayer WSe_2 revealed bandgaps of 2.2 eV for the AA stacking and 2.1 eV for other stackings, with a valence band edge shift of approximately 80 meV [Fig. 3(B)]. Additionally, constant-current STS measurements exhibited sharp peaks at specific sites, confirming the presence of flat bands, while the local density of states (LDOS) maps provided further evidence of the localization of the flat band wave function [Fig. 3(C)&(D)]. Furthermore, in a $tWSe_2$ device with a 57.5° twist angle, a distinct moiré pattern and energy bands were observed, featuring isolated flat bands and quantum-confined states [Fig. 3(E-G)]. Compared to CVD, the mechanical exfoliation approach offers enhanced controllability over the formation of superlattices. However, the undesirable coulomb screening associated with conductive substrates like graphite could still hinder the formation of many strongly correlated phases.

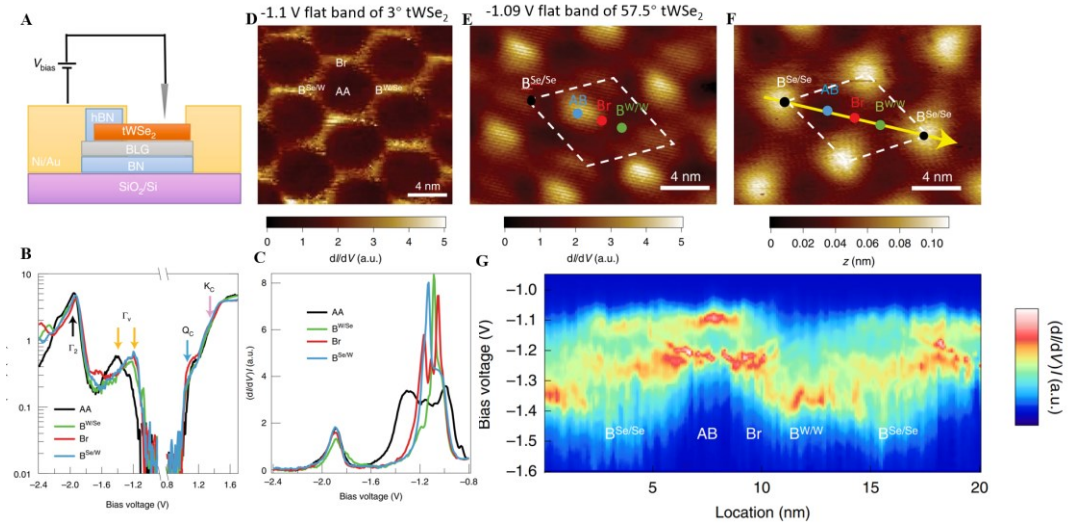

Fig. 3 (A) Schematic of the STM set-up on the $tWSe_2$ device. (B) Constant-height dI/dV versus bias voltage data, acquired at I= 100 pA, probing states in both the conduction and valence band on the four stacking alignment points for the 3° $tWSe_2$. (C) Constant-current dI/dV versus bias voltage, acquired at I= 10 pA, probing states in the valence band on the four stacking alignment points for the 3° $tWSe_2$. (D) LDOS map for the 3° $tWSe_2$ at the flat-band energy (V_{bias}=−1.1 V), acquired at I= 10 pA, featuring a conductive hexagon enclosing the insulating AA region. (E) LDOS map for the 57.5° $tWSe_2$ at the flat band, acquired at V_{bias}=−1.09 V, I= 50 pA. (F) Atomic-resolution STM topography on the 57.5° $tWSe_2$ sample. Different stacking alignment points and the unit cell are labelled in (E) and (F). (G) Constant-current dI/dV spectra along the yellow line in (F), acquired at I= 50 pA. The isolated flat band at the AB region is featured by the sharp peak around −1.1V and quantum-confined states are evidenced by the multiple sharp peaks between −1.2V and −1.3V.

To further elucidate the intricate relationship between twist angles and the electronic properties of TMD moiré patterns, in 2021, En et al. employed STM and STS to explore the twisted bilayer WSe_2 on a graphite substrate[224]. They investigated a range of twist angles, specifically 54.1°, 57°, 57.4°, 57.8°, and 58.4°, and discovered that at twist angles substantially deviating from 60°—as in the 54.1° sample—the interlayer hybridization yields only two spatially distinct flat bands with bandwidths on the order of tens of meV. However, when the twist angle approaches within 3° of 60°, lattice reconstruction occurs and, together with strong interlayer interactions, leads to the formation of triangular quantum-confined states that feature multiple energy-separated ultra-flat bands with bandwidths of just a few meV—significantly smaller than the estimated on-site Coulomb repulsion energy. These experimental results are consistent with theoretical calculations and provide a groundwork for the continued exploration of correlated phases in TMD moiré systems.

2.2 STM Studies on TMD Moiré Heterostructures on Insulating Substrates

The increasing desire for the direct visualization of correlated quantum phases in TMD moiré superlattices has spurred a growing interest in the study of TMD moiré superlattices on insulating substrates[225]. This will enable the tuning of charge carrier density in the superlattices by applying a gate voltage, a crucial step toward realizing many strongly correlated quantum phases. However, a major challenge arises from the low sample conductivity at cryogenic temperatures. The sample area located a few micrometers away from the contact electrode becomes insufficiently conductive for STM measurements. In 2021, Hongyuan, *et al.* overcame this problem and explored moiré superlattices in WSe_2/WS_2 heterostructures, utilizing hexagonal BN (hBN) as the electrically insulating substrate[226]. In this study, a comb-shaped array of graphene nanoribbons was employed as a contact electrode to apply sample bias to the mechanically fabricated TMD superlattice [Fig. 4(A-D)]. The approximately 200 nm wide TMD areas situated between two adjacent graphene nanoribbons remained unaffected by the screening and maintained sufficient conductivity even at the temperature of liquid helium. Utilizing this innovative sample structure, Hongyuan, *et al.* employed STS and ab initio simulations as investigative tools to probe and check the atomically reconstructed moiré superlattice and the consequent flat bands. Their findings revealed a pronounced 3D buckling

reconstruction and extensive in-plane strain redistribution in the WSe_2/WS_2 moiré heterostructures [Fig. 4(E-G)]. Notably, they observed a narrow, highly localized K-point moiré flat band with a mere 10meV width at the valence band edge of the heterostructure, in addition to other moiré flat bands originating from the Γ point [Fig. 4(H-M)]. Interestingly, these observations via STS challenge pre-existing theoretical models which had predicted the AA site, rather than the $B^{Se/W}$ site, as the localization of the 10 meV band. To tackle this issue, the authors conducted ab initio simulations using a calculated extensive 3D reconstructed moiré superlattice. By accounting for both in-plane strain and out-of-plane reconstruction, the theoretical simulations aligned closely with the experimental observations [Fig. 5]. Hongyuan, *et al.* concluded that the strain redistribution and 3D buckling in TMD heterostructures play a dominant role in shaping the moiré electronic structure and the corresponding moiré flat bands with low electron kinetic energy. This study thus offers critical insights into the structural and electronic properties of moiré superlattices in TMD heterostructures.

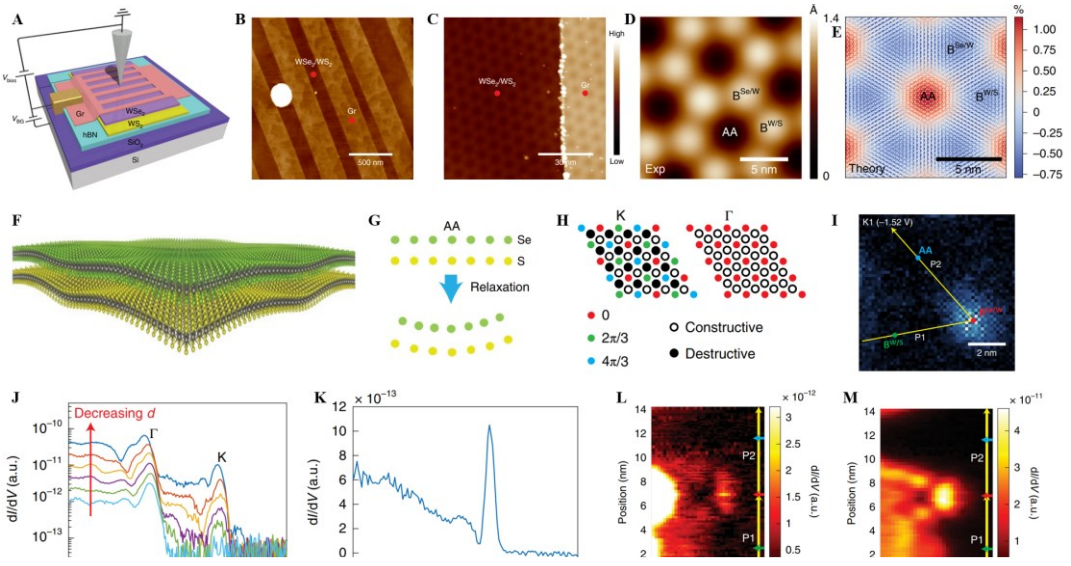

and graphene-covered area (T= 5.4 K), acquired at V_{bias}=−3 V, I= 100 pA. A moiré superlattice can be seen clearly in both areas. (D) STM image of the exposed WSe_2/WS_2 area, acquired at V_{bias}=−3V and I= 100 pA, shows a moiré period of ~8 nm. (E) Theoretical in-plane strain distribution (in %) for the WSe_2 layer from simulation. (F) 3D view of the reconstructed WSe_2/WS_2 moiré superlattice from simulation. (G) Schematic of the buckling process. (H) Illustration of the atomic-scale wavefunction interference pattern. K-point states have a 2π phase winding over the adjacent three W atoms, while Γ-point states have identical phases over all Se atom sites. (I) Large-scale dI/dV mappings of K-point states for V_{bias}=−1.52 V. The positions of $B^{Se/W}$ (red), $B^{W/S}$ (green) and AA (blue) sites are labeled here. (J) Tip–sample distance(d)-dependent STS at the $B^{Se/W}$ site, acquired at V_{bias}=−2.15 V and I= 50, 100, 200, 400, 800, 1,600 pA respectively. A second peak near V_{bias}=−1.5 V emerges with decreased d, indicating that it has a larger decay constant and originates from K-point states. (K) High-resolution dI/dV spectrum measured at the $B^{Se/W}$ site. A sharp peak with FWHM of 12 mV ± 1 mV can be observed near V_{bias}=−1.5 V.

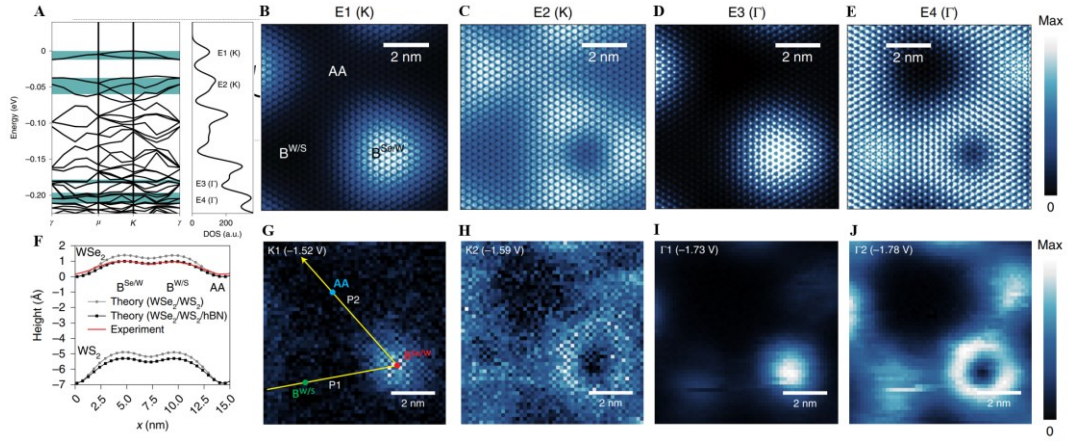

Fig. 5 (A) Calculated electronic band structure plotted in the folded mini-BZ (left) and the corresponding plot of the density of states (DOS) with 10 meV Gaussian broadening (right). Four important energy ranges (E1–E4) are labelled (green shaded areas) to highlight the topmost states folded from the K point (E1&E2) and Γ point (E3&E4). (B-E) Calculated LDOS maps. The LDOS maps are averaged over different energy ranges as labelled in (A) and over the out-of-plane direction. (F) Calculated 3D buckling of the heterostructure and comparison to experiment. Grey and black dots show the simulated positions of W atoms for a freestanding heterostructure and a heterostructure supported by hBN, respectively. (G)&(H) Large-scale dI/dV mappings of K-point states for V_{bias}=−1.52 V (G) and V_{bias}=−1.59 V (H). (I)&(J) Large-scale dI/dV mappings of Γ-point states for V_{bias}=−1.73 V (I) and V_{bias}=−1.78 V (J). Panels (B-E) and (G-J) show the same region of the sample surface. Solid dots in (G) label the positions of $B^{Se/W}$ (red), $B^{W/S}$ (green) and AA (blue) sites.

In addition to the quenched electron kinetic energy, the strong Coulomb interaction represents another critical characteristic meriting exploration within TMD moiré superlattices. Hongyuan, *et al.* have delineated a STM methodology for visualizing and manipulating the charge states of correlated electrons within a gated WS_2/WSe_2 moiré superlattice on hBN[227] [Fig. 6(A)]. They demonstrated that the local moiré sites' charge states could be imaged via their impact on the STM tunneling current at different bias, similar to the phenomena previously observed near a single molecule absorbent or a localized defect [Fig. 6(B)]. Furthermore, they successfully manipulated the charge state of correlated electrons by modulating the bias on the STM tip, leading to a localized discharge cascade within the moiré superlattice [Fig. 6(C)&(H-J)]. This innovative technique facilitated the determination of the nearest-neighbor Coulomb interaction (U_{NN}) by examining the Hamiltonian of their moiré system and discerning the

difference between the potential energy shifts induced by V_b and V_g at successive transition sites of the charge state of the ground state energy [Fig. 6(D-G)]. The on-site energy within the moiré superlattice was also ascertained by analyzing the spatial variation in the measured single-site discharge voltage. Specifically, at the midpoint between two or three neighboring moiré sites, a supplementary bias voltage is required to concurrently extract multiple electrons from these sites compared to the process of removing each electron individually. This additional energy penalty is the result from the inter-site coulomb interaction. Therefore, by modeling the local electric field at the STM junction, Hongyuan, et al. converted this bias difference into the electron-electron correlation energy. The experimental value of U_{NN} is determined as about 25meV, which is about one order of magnitude larger than the electron bandwidth determined as about 5meV previously calculated by density functional theory (DFT) and a tight-binding model, warranting a platform to host strongly correlated phases. Moreover, Hongyuan, *et al.* experimentally observed the discharging behavior on the dI/dV map of the WS_2/WSe_2 moiré superlattice and the inhomogeneity in the on-site energy influenced by a proximate point defect [Fig. 6(K-N)]. This study has successfully showcased a versatile tool for the microscopic characterization of electron properties in materials, effectively confirming the presence of strong electron-electron correlations within TMD moiré superlattices.

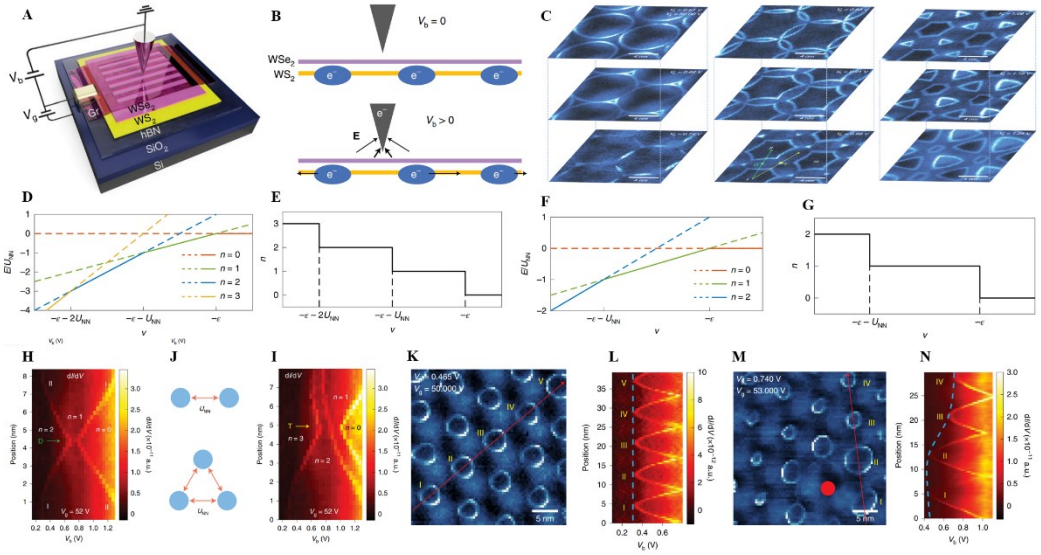

Based on the research referenced earlier, it becomes evident that within the isolated WS_2/WSe_2 moiré superlattice, the prevailing influence of long-range Coulomb interaction energy outweighs the effects of quantum fluctuations on electron motion. Consequently, this scenario leads to the anticipation of the emergence of a predicted state known as the generalized

Wigner crystal state—an orderly arrangement resembling a crystalline structure formed by electrons[49, 148, 152, 172, 228-233]. However, the direct observation of the 2D Wigner crystal lattice in real space has remained a challenge. Conventional STM, despite its high spatial resolution, can induce perturbations in the semiconducting samples due to the tip-induced band-bending referenced earlier. This could significantly affect the delicate 2D generalized Wigner crystal lattice during experimentation. To address this issue, Hongyuan, *et al.* developed a non-invasive STM spectroscopy technique in 2021, utilizing a graphene sensing layer over the WSe_2/WS_2 moiré superlattice[234]. In their experimental design, the carrier densities in the WSe_2/WS_2 moiré superlattice and the top graphene sensing layer were controlled by the top gate voltage (V_{TG}) and bottom gate voltage (V_{BG}) in their setup [Fig. 7(A)]. They determined that a V_{TG} of approximately 0.5 V is optimal as it elevates the WSe_2/WS_2 heterostructure Fermi level near the conduction band edge while maintaining the graphene sensing layer close to charge neutrality [Fig. 7(B)]. This balance allowed for higher sensitivity in imaging Wigner crystal states and minimized the screening effect on the moiré electron-electron interactions. In their experiments, they observed that the graphene layer underwent electron doping when the WSe_2/WS_2 moiré superlattice exhibited fractional filling of n=1/3, 1/2, 2/3 at the AA stacking site with V_{BG}>7V and V_{TG}=0.53V [Fig. 7(C)]. This observation indicated the presence of correlated gaps in the corresponding states in the heterostructure, rendering the WSe_2/WS_2 heterostructure electronically incompressible and forcing electrons into the graphene sensing layer. Utilizing this principle, they employed 2D dI/dV mapping of the graphene sensing layer to image the 2D electron lattice of the correlated insulating states in real space. The tunnel current between the STM tip and the graphene varies depending on the charge state of the detected moiré site. They observed a honeycomb lattice under n=2/3, a triangular lattice under n=1/3, and a stripe phase under n=1/2 [Fig. 7(D)]. To further investigate their imaging method, they examined the evolution of the n=2/3 dI/dV map with increasing bias voltage (V_{bias}) and constant gate voltages. As V_{bias} increased, the AB_1 stacking site became brighter, forming ring-like features, similar to the behavior observed under tip-induced electrical discharging [Fig. 7(E)]. This result suggests that the imaging of Wigner crystal lattices in dI/dV maps is enabled by the discharging of the moiré electron beneath the tip when V_{bias} exceeds a threshold value. This study lays a foundation for understanding Wigner crystal states in moiré heterostructures

and proposes a general approach for imaging novel correlated electron lattices in other systems.

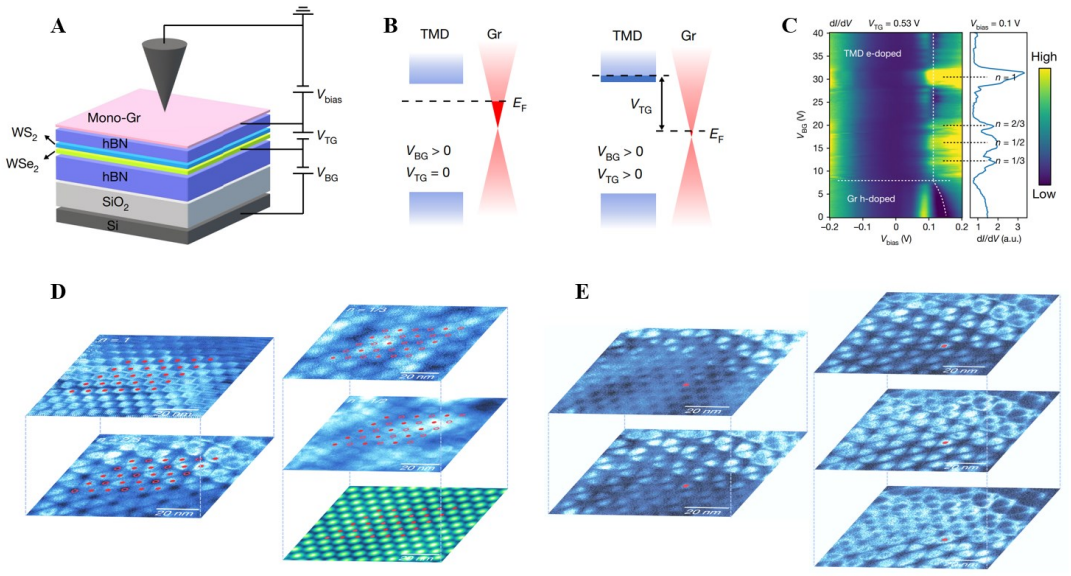

Fig. 7 (A) Schematic of the dual-gated WSe_2/WS_2 moiré heterostructure device. The top hBN thickness (5 nm) is slightly smaller than the moiré lattice constant (8 nm). Top gate (V_{TG}) and bottom gate (V_{BG}) voltages are applied to separately control the carrier density in the WSe_2/WS_2 heterostructure as well as the top graphene sensing layer. (B) Schematic of the heterostructure band alignment and Fermi levels for $V_{TG} = 0$ with $V_{BG} > 0$ and $V_{TG} > 0$ with $V_{BG} > 0$. At V_{TG}=0, the Fermi level of the WSe_2/WS_2 heterostructure is located in the bandgap while an appropriate positive V_{TG} allows the Fermi level to be lifted into the conduction band. (C) V_{BG}-dependent dI/dV spectra measured on the graphene sensing layer over an AA stacking site for $V_{TG} = 0.53$ V. Notable electron doping of the graphene layer takes place at n = 1/3, 1/2, 2/3 and 1. The tip height was set by the following parameters: $V_{bias} = -200$ mV and I = 100 pA. Right graph vertically line-cutting through the V_{BG}-dependent dI/dV spectra in left at $V_{bias} = 0.1$ V shows peaks at n = 1, 2/3, 1/2 and 1/3. (D) Upper left: dI/dV map of the n = 1 Mott insulator ($V_{bias} = 160$ mV, $V_{BG} = 30$ V, $V_{TG} = 0.53$ V); bottom left: dI/dV maps of the generalized Wigner crystal states of n = 2/3 state ($V_{bias} = 160$ mV, $V_{BG} = 21.8$ V, $V_{TG} = 0.458$ V); upper right: dI/dV maps of the generalized Wigner crystal states of n = 1/3 state ($V_{bias} = 130$ mV, $V_{BG} = 14.9$ V, $V_{TG} = 0.458$ V); middle right: dI/dV maps of the generalized Wigner crystal states of n = 1/2 state ($V_{bias} = 125$ mV, $V_{BG} = 18.7$ V, $V_{TG} = 0.458$ V); bottom right: a typical STM topographic image of the moiré superlattice shows a perfect lattice without distortion or defects. Electron-filled AB_1 sites are labelled with solid red dots and the empty AB_1 sites are labelled with open red circles. (E) Evolution of dI/dV maps for the n = 2/3 generalized Wigner crystal state with increased V_{bias} at 130mV, 145mV, 160mV, 175 mV, and 190 mV respectively from top to bottom and left to right, acquired at $V_{BG} = 21.8$ V and $V_{TG} = 0.458$ V. The red dot labels one typical electron-filled AB_1 site where a discharging ring can be observed that gets larger and brighter with increased V_{bias}.

In addition to solely relying on the tunneling electron to probe material properties, combining STM with optical excitation has also spurred the investigation of the moiré quantum phenomena related to light-matter coupling. In 2023, Hongyuan, *et al.* introduced a pioneering method termed photocurrent tunneling microscopy (PTM)[235]. This technique was devised to directly visualize the electron and hole distribution within the photoexcited in-plane charge-transfer (ICT) moiré exciton in twisted bilayer WS_2 (t-WS_2). This technique was achieved by

integrating laser excitation with STM [Fig. 8(A)]. Originating from the competition between the electron-hole Coulomb interaction and the moiré potential landscape, ICT moiré excitons own a special characteristic of producing opposing tunneling currents based on the tip's position over the exciton [Fig. 8(B)]. Utilizing this property, Hongyuan, *et al.* constructed a photocurrent map of t-WS_2 under specific conditions with a laser power of 600uW, a bias voltage (V_{bias}) of -0.60V, and a bottom gate voltage (V_{BG}) of 0 [Fig. 8(C)&(D)]. This map revealed positive photocurrents at AB sites and negative photocurrents at $B^{W/W}$ sites, providing experimental evidence for the presence of ICT moiré excitons [Fig. 8(E)]. Furthermore, both computational and experimental data presented by Hongyuan, *et al.* indicated that the bias voltage range for the coexistence of positive photocurrent at AB sites and negative photocurrent at $B^{W/W}$ sites is approximately 200mV [Fig. 8(F)]. The development of the PTM technique for the first time enables imaging of ICT moiré excitons with sub-nanometer resolution.

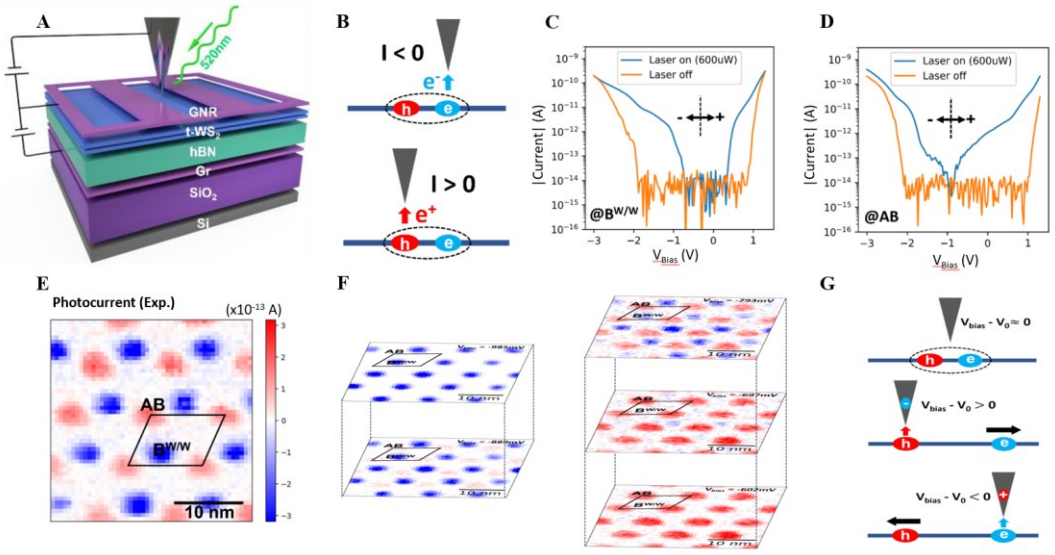

Fig. 8 (A) Sketch of experimental setup for laser-STM measurement of a near-58-degree twisted bilayer WS_2 (t-WS_2) device. The hBN and graphite substrate serve as the gate dielectric and back gate respectively. A back gate voltage V_{BG} is applied between the t-WS_2 and the graphite back gate. A graphene nanoribbon (GNR) array is placed on top of the t-WS_2 to serve as the contact electrode. A sample-tip bias V_{bias} is applied between the t-WS_2 and the STM tip to induce a tunnel current. A 520nm wavelength continuous-wave laser is focused on the tip tunnel junction. (B) Schematic for tip-position dependent tunnel current from an ICT exciton. When the STM tip sits above the electron (top panel) the larger tunnel probability for the electron yields a negative current. A positive current is detected when the tip sits above the hole (bottom panel). (C)&(D) STM tunnel current spectra measured at the (C) $B^{W/W}$ and (D) AB stacking sites with the laser turned off (orange) and on (blue). $V_{BG} = 0$. For the laser-off case, the current at both the $B^{W/W}$ and the AB sites reflect an energy gap for -2V $< V_{bias} <$ 1V. For the laser-on case (P = 600uW), photocurrent emerges in the energy gap region and the $B^{W/W}$ and AB sites show different photocurrent spectral shapes. (E) A photocurrent map of t-WS_2 measured with the laser on (P = 600uW) for V_{bias} = -0.60V and $V_{BG} = 0$ shows positive (negative) photocurrent at the AB ($B^{W/W}$) sites. (F) Evolution of t-WS_2 photocurrent maps for increasing V_{bias} at -985mV, -889mV, -793mV. -697mV, and -602mV respectively from top to bottom and left to right. Spatially alternating current polarity occurs for a V_{bias} range of ~200mV, existing only in the three V_{bias} in the middle, while negative (positive) current dominates in the lowest (highest) V_{bias}. (G) Diagrams of tip-induced ICT exciton dissociation effect, where V_0 is the bias voltage offset that compensates the work function difference between the tip and the back gate graphite. For $V_{bias} - V_0 \approx 0$, the tip does not significantly perturb the ICT exciton, hence both photocurrent polarities are seen. For $V_{bias} - V_0 > 0$, negative

3. Conclusion and Outlook

In this spotlight article, we have discussed the development of STM studies on imaging and characterizing TMD moiré superlattices. This evolution has significantly expanded our understanding of these intricate systems, through continuous innovation of device design, integration of photon excitation with STM, and meticulous research. Initially, the samples that are suitable for STM study were predominantly grown using chemical vapor deposition (CVD) on graphite substrates. This method facilitated the observation of electronic band structural influenced by the periodic moiré potential[221]. Notably, evident quantum-confined states near the band edge at stacking configurations AB^{w} and AB^{Se} were identified, corroborated by constant-height conductance maps and the NFE model[222]. However, CVD-grown samples presented challenges, including compromised sample quality and limited control over stacking order and twist angle. The use of conductive substrates further introduced strong Coulomb screening, impeding the exploration of strongly correlated phases[218-220].

To enhance sample quality, the focus shifted to mechanically exfoliated samples, offering superior control over TMD moiré pattern formation. These samples elucidated variations in electronic structures of TMD superlattices attributable to different twist angles. Initially, the exfoliated sample was transferred to a graphene substrate[223]. Addressing the conductivity challenges of TMD heterostructures at low temperatures, researchers transitioned to insulating substrates like hBN, incorporating graphene nanoribbons as contact electrodes on the top of the samples. Combining both mechanical exfoliation approach and insulating substrates, this innovative design facilitated the examination of strain redistribution and 3D buckling in TMD heterostructures, confirming the presence of strongly correlated flat bands with low electron kinetic energy[226]. Taking advantage of the strong Coulomb interaction within TMD superlattices, this new device also enabled the imaging and manipulation of correlated electron charge states by adjusting the STM tip bias[227].

Given the inherent properties of TMD moiré superlattices, including quenched electron kinetic energy and strong electron-electron correlations, the potential emergence of a generalized Wigner crystal state was expected. However, perturbations from the STM tip presented observational challenges. To get rid of such perturbations, a graphene sensing layer was introduced atop the TMD moiré pattern[234]. This layer facilitated electron transfer to graphene when the TMD heterostructure exhibited electronic incompressibility under certain fractional fillings and the bias voltage surpassed a threshold. Beyond mere tunneling electrons, optical excitations have also garnered interest in STM studies. A prime example is the measurement of photocurrent, highlighting advancements in visualizing photoexcited in-plane charge-transfer moiré excitons in TMD heterostructures by probing the opposing tunneling current across exciton sites[235].

Apart from the previously mentioned correlated phenomena, STM shows a promising future in exploring other correlated features of moiré quantum phases as well, such as the correlated insulator state[70, 148, 152, 179, 236-246] and superconductivity[122, 247-254] in TMD moiré materials. For example, the charge-transfer insulator state emerges in multiple TMD materials when on-site Coulomb repulsion dominates electron kinetic energy at one hole per superlattice site (corresponding to half-band filling)[70, 255]. This state corresponds to the freezing of the charge degree of freedom, allowing electrons only to move between anion-like and cation-like orbitals within the unit cell, to reduce on-site Coulomb repulsion[247]. Meanwhile, collective spin excitations from local magnetic moments dictate the low-energy dynamics. This phenomenon has been corroborated through temperature-dependent magnetic circular dichroism (MCD) measurements, taking advantage of the spin-valley-locked band structure and the valley-dependent optical selection rules inherent to monolayer TMDs[32, 70, 128, 150, 256]. Additionally, the spin relaxation lifetime in the charge-transfer insulator state was found to be significantly longer than that of charge excitations and further studies are needed to investigate how the persistent spin excitations from the charge-transfer insulator state can elucidate its spin configuration[148]. Aiming to reduce the overall Coulomb repulsion in TMD heterostructures at half-filling, doping with holes results in the formation of tightly-bound charge-2e excitations, known as trimers, which comprise a pair of holes bound to a charge-transfer exciton[247]. When the bandwidth of doped holes is small, the trimers form insulating pair density waves at specific doping levels, denoted as $n= 1+p/q >1$, where p and q are integers, with periodicity in alignment with the moiré lattice. As the bandwidth approximates the pair binding energy, a resonant interaction occurs between itinerant holes and charge-2e trimers, leading to unconventional superconductivity. The complexity and intrigue surrounding these correlated electron phenomena necessitate a microscopic understanding, underscoring the significant potential of STM in advancing future research.

In addition to the demonstrated successes in hard condensed matter phases, TMD moiré systems also hold significant potential in the field of chemistry [151, 181, 255, 257-260], particularly concerning charge transfer behavior. For example, recent studies have observed modification of the chemical reactivity of the moiré heterostructures, which is attributed to the interplay between the moiré potential and Coulomb interactions. In the case of WSe_2/WS_2 heterostructures with a 3° twist angle, STS detected charge transfer occurring over distances on the order of 10 nm, from MM to MX spots. This phenomenon is a consequence of increasing filling factors and the resulting rise in repulsive interaction particularly in the context of charge transfer behavior[255]. Moreover, the twist angle itself has been identified as a critical variable in modulating charge transfer kinetics within moiré patterns[257]. In the case of twisted bilayer graphene with a twist angle below 5°, the observed intrinsic electron transfer rate at AA sites, where flat bands are localized, significantly exceeds predictions made by the Gerischer-Marcus model. This significant local electrochemical enhancement is optimized near the magic angle of 1.1° and is attributed to the presence of moiré-derived highly localized flat bands and the structural relaxation of the moiré superlattice.

Looking ahead, we foresee that manipulating the moiré potential will emerge as a central strategy for both manipulating the electron correlated phenomena and enhancing chemical reactivity. Notably, many of these phenomena remain unexplored at the nanoscale, signaling the existence of a vast research frontier yet to be traversed. In this endeavor, STM is poised to

be an invaluable tool for navigating these uncharted waters with unparcelled spatial visibility.

Acknowledgement

This material is based upon work supported by the National Science Foundation under Grant CHE-2303936.

References:

1. Gong, C.; Li, L.; Li, Z.; Ji, H.; Stern, A.; Xia, Y.; Cao, T.; Bao, W.; Wang, C.; Wang, Y.; Qiu, Z. Q.; Cava, R. J.; Louie, S. G.; Xia, J.; Zhang, X., Discovery of intrinsic ferromagnetism in two-dimensional van der Waals crystals. *Nature* **2017,** *546* (7657), 265-269.

2. Bonilla, M.; Kolekar, S.; Ma, Y.; Diaz, H. C.; Kalappattil, V.; Das, R.; Eggers, T.; Gutierrez, H. R.; Phan, M.-H.; Batzill, M., Strong room-temperature ferromagnetism in VSe2 monolayers on van der Waals substrates. *Nature Nanotechnology* **2018,** *13* (4), 289-293.

3. Khan, Y.; Obaidulla, S. M.; Habib, M. R.; Gayen, A.; Liang, T.; Wang, X.; Xu, M., Recent breakthroughs in two-dimensional van der Waals magnetic materials and emerging applications. *Nano Today* **2020,** *34*, 100902.

4. Fang, M.; Yang, E.-H. Advances in Two-Dimensional Magnetic Semiconductors via Substitutional Doping of Transition Metal Dichalcogenides *Materials* [Online], 2023.

5. Cai, L.; He, J.; Liu, Q.; Yao, T.; Chen, L.; Yan, W.; Hu, F.; Jiang, Y.; Zhao, Y.; Hu, T.; Sun, Z.; Wei, S., Vacancy-Induced Ferromagnetism of MoS2 Nanosheets. *Journal of the American Chemical Society* **2015,** *137* (7), 2622-2627.

6. Guo, Y.; Dai, J.; Zhao, J.; Wu, C.; Li, D.; Zhang, L.; Ning, W.; Tian, M.; Zeng, X. C.; Xie, Y., Large Negative Magnetoresistance Induced by Anionic Solid Solutions in Two-Dimensional Spin-Frustrated Transition Metal Chalcogenides. *Physical Review Letters* **2014,** *113* (15), 157202.

7. Zhang, Z.; Zou, X.; Crespi, V. H.; Yakobson, B. I., Intrinsic Magnetism of Grain Boundaries in Two-Dimensional Metal Dichalcogenides. *ACS Nano* **2013,** *7* (12), 10475-10481.

8. Zhang, J.; Soon, J. M.; Loh, K. P.; Yin, J.; Ding, J.; Sullivian, M. B.; Wu, P., Magnetic Molybdenum Disulfide Nanosheet Films. *Nano Letters* **2007,** *7* (8), 2370-2376.

9. Yun, W. S.; Lee, J. D., Strain-Induced Magnetism in Single-Layer MoS2: Origin and Manipulation. *The Journal of Physical Chemistry C* **2015,** *119* (5), 2822-2827.

10. Tongay, S.; Varnoosfaderani, S. S.; Appleton, B. R.; Wu, J.; Hebard, A. F. J. A. P. L., Magnetic properties of MoS2: Existence of ferromagnetism. **2012,** *101* (12).

11. Mishra, R.; Zhou, W.; Pennycook, S. J.; Pantelides, S. T.; Idrobo, J.-C., Long-range ferromagnetic ordering in manganese-doped two-dimensional dichalcogenides. *Physical Review B* **2013,** *88* (14), 144409.

12. Roch, J. G.; Froehlicher, G.; Leisgang, N.; Makk, P.; Watanabe, K.; Taniguchi, T.; Warburton, R. J., Spin-polarized electrons in monolayer MoS2. *Nature Nanotechnology* **2019,** *14* (5), 432-436.

13. Movva, H. C. P.; Fallahazad, B.; Kim, K.; Larentis, S.; Taniguchi, T.; Watanabe, K.; Banerjee, S. K.; Tutuc, E., Density-Dependent Quantum Hall States and Zeeman Splitting in Monolayer and Bilayer WSe2. *Physical Review Letters* **2017,** *118* (24), 247701.

14. Ishii, S.; Yokoshi, N.; Ishihara, H., Optical selection rule of monolayer transition metal

dichalcogenide by an optical vortex. *Journal of Physics: Conference Series* **2019,** *1220* (1), 012056.
15. Mak, K. F.; Shan, J., Photonics and optoelectronics of 2D semiconductor transition metal dichalcogenides. *Nature Photonics* **2016,** *10* (4), 216-226.
16. Yang, X.; Li, B., Monolayer MoS2 for nanoscale photonics. **2020,** *9* (7), 1557-1577.
17. Shi, H.; Pan, H.; Zhang, Y.-W.; Yakobson, B. I., Quasiparticle band structures and optical properties of strained monolayer MoS2 and WS2. *Physical Review B* **2013,** *87* (15), 155304.
18. Gutiérrez, H. R.; Perea-López, N.; Elías, A. L.; Berkdemir, A.; Wang, B.; Lv, R.; López-Urías, F.; Crespi, V. H.; Terrones, H.; Terrones, M., Extraordinary Room-Temperature Photoluminescence in Triangular WS2 Monolayers. *Nano Letters* **2013,** *13* (8), 3447-3454.
19. Zeng, H.; Liu, G.-B.; Dai, J.; Yan, Y.; Zhu, B.; He, R.; Xie, L.; Xu, S.; Chen, X.; Yao, W.; Cui, X., Optical signature of symmetry variations and spin-valley coupling in atomically thin tungsten dichalcogenides. *Scientific Reports* **2013,** *3* (1), 1608.
20. Choi, W.; Akhtar, I.; Rehman, M. A.; Kim, M.; Kang, D.; Jung, J.; Myung, Y.; Kim, J.; Cheong, H.; Seo, Y., Twist-Angle-Dependent Optoelectronics in a Few-Layer Transition-Metal Dichalcogenide Heterostructure. *ACS Applied Materials & Interfaces* **2019,** *11* (2), 2470-2478.
21. Mak, K. F.; He, K.; Shan, J.; Heinz, T. F., Control of valley polarization in monolayer MoS2 by optical helicity. *Nature Nanotechnology* **2012,** *7* (8), 494-498.
22. Sallen, G.; Bouet, L.; Marie, X.; Wang, G.; Zhu, C. R.; Han, W. P.; Lu, Y.; Tan, P. H.; Amand, T.; Liu, B. L.; Urbaszek, B., Robust optical emission polarization in MoS2 monolayers through selective valley excitation. *Physical Review B* **2012,** *86* (8), 081301.
23. Korn, T.; Heydrich, S.; Hirmer, M.; Schmutzler, J.; Schüller, C., Low-temperature photocarrier dynamics in monolayer MoS2. *Applied Physics Letters* **2011,** *99*, 2109-2109.
24. Splendiani, A.; Sun, L.; Zhang, Y.; Li, T.; Kim, J.; Chim, C.-Y.; Galli, G.; Wang, F., Emerging Photoluminescence in Monolayer MoS2. *Nano Letters* **2010,** *10* (4), 1271-1275.
25. Lopez-Sanchez, O.; Lembke, D.; Kayci, M.; Radenovic, A.; Kis, A., Ultrasensitive photodetectors based on monolayer MoS2. *Nature Nanotechnology* **2013,** *8* (7), 497-501.
26. Zeng, H.; Dai, J.; Yao, W.; Xiao, D.; Cui, X., Valley polarization in MoS2 monolayers by optical pumping. *Nature Nanotechnology* **2012,** *7* (8), 490-493.
27. Lee, H. S.; Min, S.-W.; Chang, Y.-G.; Park, M. K.; Nam, T.; Kim, H.; Kim, J. H.; Ryu, S.; Im, S., MoS2 Nanosheet Phototransistors with Thickness-Modulated Optical Energy Gap. *Nano Letters* **2012,** *12* (7), 3695-3700.
28. Beal, A. R.; Hughes, H. P.; Liang, W. Y., The reflectivity spectra of some group VA transition metal dichalcogenides. *Journal of Physics C: Solid State Physics* **1975,** *8* (24), 4236.
29. Deng, W.; Zheng, Z.; Li, J.; Zhou, R.; Chen, X.; Zhang, D.; Lu, Y.; Wang, C.; You, C.; Li, S.; Sun, L.; Wu, Y.; Li, X.; An, B.; Liu, Z.; Wang, Q. j.; Duan, X.; Zhang, Y., Electrically tunable two-dimensional heterojunctions for miniaturized near-infrared spectrometers. *Nature Communications* **2022,** *13* (1), 4627.
30. Mak, K. F.; Lee, C.; Hone, J.; Shan, J.; Heinz, T. F., Atomically Thin MoS2: A New Direct-Gap Semiconductor. *Physical Review Letters* **2010,** *105* (13), 136805.
31. Cao, T.; Wang, G.; Han, W.; Ye, H.; Zhu, C.; Shi, J.; Niu, Q.; Tan, P.; Wang, E.; Liu, B.; Feng, J., Valley-selective circular dichroism of monolayer molybdenum disulphide. *Nature Communications* **2012,** *3* (1), 887.
32. Xiao, D.; Liu, G.-B.; Feng, W.; Xu, X.; Yao, W., Coupled Spin and Valley Physics in Monolayers of MoS2 and Other Group-VI Dichalcogenides. *Physical Review Letters* **2012,** *108* (19), 196802.

33. Xu, X.; Yao, W.; Xiao, D.; Heinz, T. F., Spin and pseudospins in layered transition metal dichalcogenides. *Nature Physics* **2014,** *10* (5), 343-350.
34. Coehoorn, R.; Haas, C.; de Groot, R. A., Electronic structure of MoSe2, MoS2, and WSe2. II. The nature of the optical band gaps. *Physical Review B* **1987,** *35* (12), 6203-6206.
35. Mak, K. F.; McGill, K. L.; Park, J.; McEuen, P. L., The valley Hall effect in MoS2 transistors. *Science* **2014,** *344* (6191), 1489-1492.
36. Wang, Q. H.; Kalantar-Zadeh, K.; Kis, A.; Coleman, J. N.; Strano, M. S., Electronics and optoelectronics of two-dimensional transition metal dichalcogenides. *Nature Nanotechnology* **2012,** *7* (11), 699-712.
37. Manzeli, S.; Ovchinnikov, D.; Pasquier, D.; Yazyev, O. V.; Kis, A., 2D transition metal dichalcogenides. *Nature Reviews Materials* **2017,** *2* (8), 17033.
38. Radisavljevic, B.; Radenovic, A.; Brivio, J.; Giacometti, V.; Kis, A., Single-layer MoS2 transistors. *Nature Nanotechnology* **2011,** *6* (3), 147-150.
39. Zhao, W.; Ghorannevis, Z.; Chu, L.; Toh, M.; Kloc, C.; Tan, P.-H.; Eda, G., Evolution of Electronic Structure in Atomically Thin Sheets of WS2 and WSe2. *ACS Nano* **2013,** *7* (1), 791-797.
40. Fang, H.; Chuang, S.; Chang, T. C.; Takei, K.; Takahashi, T.; Javey, A., High-Performance Single Layered WSe2 p-FETs with Chemically Doped Contacts. *Nano Letters* **2012,** *12* (7), 3788-3792.
41. Kim, S.; Konar, A.; Hwang, W.-S.; Lee, J. H.; Lee, J.; Yang, J.; Jung, C.; Kim, H.; Yoo, J.-B.; Choi, J.-Y.; Jin, Y. W.; Lee, S. Y.; Jena, D.; Choi, W.; Kim, K., High-mobility and low-power thin-film transistors based on multilayer MoS2 crystals. *Nature Communications* **2012,** *3* (1), 1011.
42. Tongay, S.; Zhou, J.; Ataca, C.; Lo, K.; Matthews, T. S.; Li, J.; Grossman, J. C.; Wu, J., Thermally Driven Crossover from Indirect toward Direct Bandgap in 2D Semiconductors: MoSe2 versus MoS2. *Nano Letters* **2012,** *12* (11), 5576-5580.
43. Qian, X.; Liu, J.; Fu, L.; Li, J., Quantum spin Hall effect in two-dimensional transition metal dichalcogenides. *Science* **2014,** *346* (6215), 1344-1347.
44. Jiang, Y.; Chen, S.; Zheng, W.; Zheng, B.; Pan, A., Interlayer exciton formation, relaxation, and transport in TMD van der Waals heterostructures. *Light: Science & Applications* **2021,** *10* (1), 72.
45. Brem, S.; Lin, K.-Q.; Gillen, R.; Bauer, J. M.; Maultzsch, J.; Lupton, J. M.; Malic, E. J. N., Hybridized intervalley moiré excitons and flat bands in twisted WSe2 bilayers. **2020**.
46. He, K.; Poole, C.; Mak, K. F.; Shan, J., Experimental Demonstration of Continuous Electronic Structure Tuning via Strain in Atomically Thin MoS2. *Nano Letters* **2013,** *13* (6), 2931-2936.
47. Huang, Y. L.; Chen, Y.; Zhang, W.; Quek, S. Y.; Chen, C.-H.; Li, L.-J.; Hsu, W.-T.; Chang, W.-H.; Zheng, Y. J.; Chen, W.; Wee, A. T. S., Bandgap tunability at single-layer molybdenum disulphide grain boundaries. *Nature Communications* **2015,** *6* (1), 6298.
48. Radisavljevic, B.; Kis, A., Mobility engineering and a metal–insulator transition in monolayer MoS2. *Nature Materials* **2013,** *12* (9), 815-820.
49. Jin, C.; Tao, Z.; Li, T.; Xu, Y.; Tang, Y.; Zhu, J.; Liu, S.; Watanabe, K.; Taniguchi, T.; Hone, J. C.; Fu, L.; Shan, J.; Mak, K. F., Stripe phases in WSe2/WS2 moiré superlattices. *Nature Materials* **2021,** *20* (7), 940-944.
50. Zhou, W.; Zou, X.; Najmaei, S.; Liu, Z.; Shi, Y.; Kong, J.; Lou, J.; Ajayan, P. M.; Yakobson, B. I.; Idrobo, J.-C., Intrinsic Structural Defects in Monolayer Molybdenum Disulfide. *Nano Letters* **2013,** *13* (6), 2615-2622.
51. Coleman, J. N.; Lotya, M.; O'Neill, A.; Bergin, S. D.; King, P. J.; Khan, U.; Young, K.; Gaucher, A.; De, S.; Smith, R. J.; Shvets, I. V.; Arora, S. K.; Stanton, G.; Kim, H.-Y.; Lee, K.; Kim, G. T.;

Duesberg, G. S.; Hallam, T.; Boland, J. J.; Wang, J. J.; Donegan, J. F.; Grunlan, J. C.; Moriarty, G.; Shmeliov, A.; Nicholls, R. J.; Perkins, J. M.; Grieveson, E. M.; Theuwissen, K.; McComb, D. W.; Nellist, P. D.; Nicolosi, V., Two-Dimensional Nanosheets Produced by Liquid Exfoliation of Layered Materials. *Science* **2011,** *331* (6017), 568-571.

52. Li, H.; Wu, J.; Yin, Z.; Zhang, H., Preparation and Applications of Mechanically Exfoliated Single-Layer and Multilayer MoS2 and WSe2 Nanosheets. *Accounts of Chemical Research* **2014,** *47* (4), 1067-1075.

53. Zhang, X.; Lai, Z.; Tan, C.; Zhang, H., Solution-Processed Two-Dimensional MoS2 Nanosheets: Preparation, Hybridization, and Applications. *Angewandte Chemie (International ed. in English)* **2016,** *55*.

54. Zhang, Y.; Yao, Y.; Sendeku, M. G.; Yin, L.; Zhan, X.; Wang, F.; Wang, Z.; He, J. J. A. M., Recent Progress in CVD Growth of 2D Transition Metal Dichalcogenides and Related Heterostructures. **2019,** *31*.

55. Xia, J.; Yan, J.; Wang, Z.; He, Y.; Gong, Y.; Chen, W.; Sum, T. C.; Liu, Z.; Ajayan, P. M.; Shen, Z., Strong coupling and pressure engineering in WSe2–MoSe2 heterobilayers. *Nature Physics* **2021,** *17* (1), 92-98.

56. Lin, Z.; McCreary, A.; Briggs, N.; Subramanian, S.; Zhang, K.; Sun, Y.; Li, X.; Borys, N. J.; Yuan, H.; Fullerton-Shirey, S. K.; Chernikov, A.; Zhao, H.; McDonnell, S.; Lindenberg, A. M.; Xiao, K.; LeRoy, B. J.; Drndić, M.; Hwang, J. C. M.; Park, J.; Chhowalla, M.; Schaak, R. E.; Javey, A.; Hersam, M. C.; Robinson, J.; Terrones, M., 2D materials advances: from large scale synthesis and controlled heterostructures to improved characterization techniques, defects and applications. *2D Materials* **2016,** *3* (4), 042001.

57. Huang, X.; Han, X.; Dai, Y.; Xu, X.; Yan, J.; Huang, M.; Ding, P.; Zhang, D.; Chen, H.; Laxmi, V.; Wu, X.; Liu, L.; Wang, Y.; Xu, Y.; Huang, Y., Recent progress on fabrication and flat-band physics in 2D transition metal dichalcogenides moiré superlattices. *Journal of Semiconductors* **2023,** *44* (1), 011901.

58. Wang, L.; Meric, I.; Huang, P. Y.; Gao, Q.; Gao, Y.; Tran, H.; Taniguchi, T.; Watanabe, K.; Campos, L. M.; Muller, D. A.; Guo, J.; Kim, P.; Hone, J.; Shepard, K. L.; Dean, C. R., One-Dimensional Electrical Contact to a Two-Dimensional Material. *Science* **2013,** *342* (6158), 614-617.

59. Cao, Y.; Fatemi, V.; Demir, A.; Fang, S.; Tomarken, S. L.; Luo, J. Y.; Sanchez-Yamagishi, J. D.; Watanabe, K.; Taniguchi, T.; Kaxiras, E.; Ashoori, R. C.; Jarillo-Herrero, P., Correlated insulator behaviour at half-filling in magic-angle graphene superlattices. *Nature* **2018,** *556* (7699), 80-84.

60. Cao, Y.; Fatemi, V.; Fang, S.; Watanabe, K.; Taniguchi, T.; Kaxiras, E.; Jarillo-Herrero, P., Unconventional superconductivity in magic-angle graphene superlattices. *Nature* **2018,** *556* (7699), 43-50.

61. Dean, C.; Wang, L.; Maher, P.; Forsythe, C.; Ghahari, F.; Gao, Y.; Katoch, J.; Ishigami, M.; Moon, P.; Koshino, M.; Taniguchi, T.; Watanabe, K.; Shepard, K.; Hone, J.; Kim, P., Hofstadter's butterfly and the fractal quantum Hall effect in Moire superlattices. *Nature* **2013,** *497*, 598.

62. Hunt, B.; Sanchez-Yamagishi, J. D.; Young, A. F.; Yankowitz, M.; LeRoy, B. J.; Watanabe, K.; Taniguchi, T.; Moon, P.; Koshino, M.; Jarillo-Herrero, P.; Ashoori, R. C., Massive Dirac Fermions and Hofstadter Butterfly in a van der Waals Heterostructure. *Science* **2013,** *340* (6139), 1427-1430.

63. Jiang, Y.; Lai, X.; Watanabe, K.; Taniguchi, T.; Haule, K.; Mao, J.; Andrei, E., Charge-order and broken rotational symmetry in magic angle twisted bilayer graphene. *Nature* **2019,** *573*, 1.

64. Kerelsky, A.; McGilly, L. J.; Kennes, D. M.; Xian, L.; Yankowitz, M.; Chen, S.; Watanabe, K.;

Taniguchi, T.; Hone, J.; Dean, C.; Rubio, A.; Pasupathy, A. N., Maximized electron interactions at the magic angle in twisted bilayer graphene. *Nature* **2019,** *572* (7767), 95-100.

65. Ponomarenko, L. A.; Gorbachev, R. V.; Yu, G. L.; Elias, D. C.; Jalil, R.; Patel, A. A.; Mishchenko, A.; Mayorov, A. S.; Woods, C. R.; Wallbank, J. R.; Mucha-Kruczynski, M.; Piot, B. A.; Potemski, M.; Grigorieva, I. V.; Novoselov, K. S.; Guinea, F.; Fal'ko, V. I.; Geim, A. K., Cloning of Dirac fermions in graphene superlattices. *Nature* **2013,** *497* (7451), 594-597.

66. Xie, Y.; Lian, B.; Jäck, B.; Liu, X.; Chiu, C.-L.; Watanabe, K.; Taniguchi, T.; Bernevig, B. A.; Yazdani, A., Spectroscopic signatures of many-body correlations in magic-angle twisted bilayer graphene. *Nature* **2019,** *572* (7767), 101-105.

67. Yankowitz, M.; Xue, J.; Cormode, D.; Sanchez-Yamagishi, J. D.; Watanabe, K.; Taniguchi, T.; Jarillo-Herrero, P.; Jacquod, P.; LeRoy, B. J., Emergence of superlattice Dirac points in graphene on hexagonal boron nitride. *Nature Physics* **2012,** *8* (5), 382-386.

68. Yoo, H.; Engelke, R.; Carr, S.; Fang, S.; Zhang, K.; Cazeaux, P.; Sung, S. H.; Hovden, R.; Tsen, A. W.; Taniguchi, T.; Watanabe, K.; Yi, G.-C.; Kim, M.; Luskin, M.; Tadmor, E. B.; Kaxiras, E.; Kim, P., Atomic and electronic reconstruction at the van der Waals interface in twisted bilayer graphene. *Nature Materials* **2019,** *18* (5), 448-453.

69. Magorrian, S. J.; Enaldiev, V. V.; Zólyomi, V.; Ferreira, F.; Fal'ko, V. I.; Ruiz-Tijerina, D. A., Multifaceted moire superlattice physics in twisted WSe2 bilayers. *Physical Review B* **2021,** *104* (12), 125440.

70. Mak, K. F.; Shan, J., Semiconductor moiré materials. *Nature Nanotechnology* **2022,** *17* (7), 686-695.

71. McGilly, L. J.; Kerelsky, A.; Finney, N. R.; Shapovalov, K.; Shih, E.-M.; Ghiotto, A.; Zeng, Y.; Moore, S. L.; Wu, W.; Bai, Y.; Watanabe, K.; Taniguchi, T.; Stengel, M.; Zhou, L.; Hone, J.; Zhu, X.; Basov, D. N.; Dean, C.; Dreyer, C. E.; Pasupathy, A. N., Visualization of moiré superlattices. *Nature Nanotechnology* **2020,** *15* (7), 580-584.

72. Halbertal, D.; Finney, N. R.; Sunku, S. S.; Kerelsky, A.; Rubio-Verdú, C.; Shabani, S.; Xian, L.; Carr, S.; Chen, S.; Zhang, C.; Wang, L.; Gonzalez-Acevedo, D.; McLeod, A. S.; Rhodes, D.; Watanabe, K.; Taniguchi, T.; Kaxiras, E.; Dean, C. R.; Hone, J. C.; Pasupathy, A. N.; Kennes, D. M.; Rubio, A.; Basov, D. N., Moiré metrology of energy landscapes in van der Waals heterostructures. *Nature Communications* **2021,** *12* (1), 242.

73. Kim, K.; DaSilva, A.; Huang, S.; Fallahazad, B.; Larentis, S.; Taniguchi, T.; Watanabe, K.; LeRoy, B.; Macdonald, A.; Tutuc, E., Tunable Moire Bands and Strong Correlations in Small-Twist-Angle Bilayer Graphene. *Proceedings of the National Academy of Sciences* **2017,** *114*.

74. Utama, M. I. B.; Koch, R. J.; Lee, K.; Leconte, N.; Li, H.; Zhao, S.; Jiang, L.; Zhu, J.; Watanabe, K.; Taniguchi, T.; Ashby, P. D.; Weber-Bargioni, A.; Zettl, A.; Jozwiak, C.; Jung, J.; Rotenberg, E.; Bostwick, A.; Wang, F. J. N. P., Visualization of the flat electronic band in twisted bilayer graphene near the magic angle twist. **2019,** *17*, 184 - 188.

75. Jones, A. J. H.; Muzzio, R.; Majchrzak, P. E.; Pakdel, S.; Curcio, D.; Volckaert, K.; Biswas, D.; Gobbo, J.; Singh, S.; Robinson, J. T.; Watanabe, K.; Taniguchi, T.; Kim, T. K.; Cacho, C.; Lanatà, N.; Miwa, J. A.; Hofmann, P.; Katoch, J.; Ulstrup, S. J. A. M., Observation of Electrically Tunable van Hove Singularities in Twisted Bilayer Graphene from NanoARPES. **2020,** *32*.

76. Lisi, S.; Lu, X.; Benschop, T.; de Jong, T. A.; Stepanov, P.; Duran, J. R.; Margot, F.; Cucchi, I.; Cappelli, E.; Hunter, A.; Tamai, A.; Kandyba, V.; Giampietri, A.; Barinov, A.; Jobst, J.; Stalman, V.; Leeuwenhoek, M.; Watanabe, K.; Taniguchi, T.; Rademaker, L.; van der Molen, S. J.; Allan, M. P.;

Efetov, D. K.; Baumberger, F., Observation of flat bands in twisted bilayer graphene. *Nature Physics* **2021,** *17* (2), 189-193.

77. Li, G.; Luican, A.; Lopes dos Santos, J. M. B.; Castro Neto, A. H.; Reina, A.; Kong, J.; Andrei, E. Y., Observation of Van Hove singularities in twisted graphene layers. *Nature Physics* **2010,** *6* (2), 109-113.

78. Brihuega, I.; Mallet, P.; González-Herrero, H.; Trambly de Laissardière, G.; Ugeda, M. M.; Magaud, L.; Gómez-Rodríguez, J. M.; Ynduráin, F.; Veuillen, J. Y., Unraveling the Intrinsic and Robust Nature of van Hove Singularities in Twisted Bilayer Graphene by Scanning Tunneling Microscopy and Theoretical Analysis. *Physical Review Letters* **2012,** *109* (19), 196802.

79. Wong, D.; Wang, Y.; Jung, J.; Pezzini, S.; DaSilva, A. M.; Tsai, H.-Z.; Jung, H. S.; Khajeh, R.; Kim, Y.; Lee, J.; Kahn, S.; Tollabimazraehno, S.; Rasool, H.; Watanabe, K.; Taniguchi, T.; Zettl, A.; Adam, S.; MacDonald, A. H.; Crommie, M. F., Local spectroscopy of moire-induced electronic structure in gate-tunable twisted bilayer graphene. *Physical Review B* **2015,** *92* (15), 155409.

80. Choi, Y.; Kemmer, J.; Peng, Y.; Thomson, A.; Arora, H.; Polski, R.; Zhang, Y.; Ren, H.; Alicea, J.; Refael, G.; von Oppen, F.; Watanabe, K.; Taniguchi, T.; Nadj-Perge, S., Electronic correlations in twisted bilayer graphene near the magic angle. *Nature Physics* **2019,** *15* (11), 1174-1180.

81. Wu, F.; Lovorn, T.; Tutuc, E.; MacDonald, A. H., Hubbard Model Physics in Transition Metal Dichalcogenide Moire Bands. *Physical Review Letters* **2018,** *121* (2), 026402.

82. Naik, M. H.; Jain, M., Ultraflatbands and Shear Solitons in Moire Patterns of Twisted Bilayer Transition Metal Dichalcogenides. *Physical Review Letters* **2018,** *121* (26), 266401.

83. Gatti, G.; Issing, J.; Rademaker, L.; Margot, F.; de Jong, T. A.; van der Molen, S. J.; Teyssier, J.; Kim, T. K.; Watson, M. D.; Cacho, C.; Dudin, P.; Avila, J.; Edwards, K. C.; Paruch, P.; Ubrig, N.; Gutiérrez-Lezama, I.; Morpurgo, A. F.; Tamai, A.; Baumberger, F., Flat Gamma Moire Bands in Twisted Bilayer WSe2. *Physical Review Letters* **2023,** *131* (4), 046401.

84. Moosa, A. A.; Abed, M. S. J. T. J. o. C., Graphene preparation and graphite exfoliation. **2021,** *45*, 493 - 519.

85. Stankovich, S.; Dikin, D. A.; Piner, R. D.; Kohlhaas, K. A.; Kleinhammes, A.; Jia, Y.; Wu, Y.; Nguyen, S. T.; Ruoff, R. S., Synthesis of graphene-based nanosheets via chemical reduction of exfoliated graphite oxide. *Carbon* **2007,** *45* (7), 1558-1565.

86. Li, X.; Cai, W.; An, J.; Kim, S.; Nah, J.; Yang, D.; Piner, R.; Velamakanni, A.; Jung, I.; Tutuc, E.; Banerjee, S. K.; Colombo, L.; Ruoff, R. S., Large-Area Synthesis of High-Quality and Uniform Graphene Films on Copper Foils. *Science* **2009,** *324* (5932), 1312-1314.

87. Kim, K. S.; Zhao, Y.; Jang, H.; Lee, S. Y.; Kim, J. M.; Kim, K. S.; Ahn, J.-H.; Kim, P.; Choi, J.-Y.; Hong, B. H., Large-scale pattern growth of graphene films for stretchable transparent electrodes. *Nature* **2009,** *457* (7230), 706-710.

88. Hernandez, Y.; Nicolosi, V.; Lotya, M.; Blighe, F. M.; Sun, Z.; De, S.; McGovern, I. T.; Holland, B.; Byrne, M.; Gun'Ko, Y. K.; Boland, J. J.; Niraj, P.; Duesberg, G.; Krishnamurthy, S.; Goodhue, R.; Hutchison, J.; Scardaci, V.; Ferrari, A. C.; Coleman, J. N., High-yield production of graphene by liquid-phase exfoliation of graphite. *Nature Nanotechnology* **2008,** *3* (9), 563-568.

89. Park, S.; Ruoff, R. S., Chemical methods for the production of graphenes. *Nature Nanotechnology* **2009,** *4* (4), 217-224.

90. Cai, M.; Thorpe, D.; Adamson, D. H.; Schniepp, H. C., Methods of graphite exfoliation. *Journal of Materials Chemistry* **2012,** *22* (48), 24992-25002.

91. Tiwari, S. K.; Huczko, A.; Oraon, R.; De Adhikari, A.; Nayak, G. C., Facile electrochemical

synthesis of few layered graphene from discharged battery electrode and its application for energy storage. *Arabian Journal of Chemistry* **2017,** *10* (4), 556-565.

92. Yi, M.; Shen, Z., A review on mechanical exfoliation for the scalable production of graphene. *Journal of Materials Chemistry A* **2015,** *3* (22), 11700-11715.

93. Liu, L.; Shen, Z.; Yi, M.; Zhang, X.; Ma, S., A green, rapid and size-controlled production of high-quality graphene sheets by hydrodynamic forces. *RSC Advances* **2014,** *4* (69), 36464-36470.

94. Zhang, Y.; Zhang, L.; Zhou, C., Review of Chemical Vapor Deposition of Graphene and Related Applications. *Accounts of Chemical Research* **2013,** *46* (10), 2329-2339.

95. Lomer, W. M., The Valence Bands in Two-Dimensional Graphite. *Proceedings of the Royal Society of London. Series A, Mathematical and Physical Sciences* **1955,** *227* (1170), 330-349.

96. Slonczewski, J. C.; Weiss, P. R., Band Structure of Graphite. *Physical Review* **1958,** *109* (2), 272-279.

97. Dresselhaus, G.; Dresselhaus, M. S., Spin-Orbit Interaction in Graphite. *Physical Review* **1965,** *140* (1A), A401-A412.

98. Bassani, F.; Parravicini, G. P., Band structure and optical properties of graphite and of the layer compounds GaS and GaSe. *Il Nuovo Cimento B (1965-1970)* **1967,** *50* (1), 95-128.

99. Mañes, J. L., Existence of bulk chiral fermions and crystal symmetry. *Physical Review B* **2012,** *85* (15), 155118.

100. Kogan, E.; Nazarov, V. U., Symmetry classification of energy bands in graphene. *Physical Review B* **2012,** *85* (11), 115418.

101. Sun, L.; Rademaker, L.; Mauro, D.; Scarfato, A.; Pásztor, Á.; Gutiérrez-Lezama, I.; Wang, Z.; Martinez-Castro, J.; Morpurgo, A. F.; Renner, C., Determining spin-orbit coupling in graphene by quasiparticle interference imaging. *Nature Communications* **2023,** *14* (1), 3771.

102. Avsar, A.; Tan, J. Y.; Taychatanapat, T.; Balakrishnan, J.; Koon, G. K. W.; Yeo, Y.; Lahiri, J.; Carvalho, A.; Rodin, A. S.; O'Farrell, E. C. T.; Eda, G.; Castro Neto, A. H.; Özyilmaz, B., Spin–orbit proximity effect in graphene. *Nature Communications* **2014,** *5* (1), 4875.

103. Wang, Z.; Ki, D.-K.; Khoo, J. Y.; Mauro, D.; Berger, H.; Levitov, L. S.; Morpurgo, A. F., Origin and Magnitude of `Designer' Spin-Orbit Interaction in Graphene on Semiconducting Transition Metal Dichalcogenides. *Physical Review X* **2016,** *6* (4), 041020.

104. Island, J. O.; Cui, X.; Lewandowski, C.; Khoo, J. Y.; Spanton, E. M.; Zhou, H.; Rhodes, D.; Hone, J. C.; Taniguchi, T.; Watanabe, K.; Levitov, L. S.; Zaletel, M. P.; Young, A. F., Spin–orbit-driven band inversion in bilayer graphene by the van der Waals proximity effect. *Nature* **2019,** *571* (7763), 85-89.

105. Koh, J. M.; Alicea, J.; Lantagne-Hurtubise, E. In *Correlated Phases in Spin-Orbit-Coupled Rhombohedral Trilayer Graphene*, 2023.

106. Wang, D.; Che, S.; Cao, G.; Lyu, R.; Watanabe, K.; Taniguchi, T.; Lau, C. N.; Bockrath, M., Quantum Hall Effect Measurement of Spin–Orbit Coupling Strengths in Ultraclean Bilayer Graphene/WSe2 Heterostructures. *Nano Letters* **2019,** *19* (10), 7028-7034.

107. Novoselov, K. S.; Geim, A. K.; Morozov, S. V.; Jiang, D.; Zhang, Y.; Dubonos, S. V.; Grigorieva, I. V.; Firsov, A. A., Electric Field Effect in Atomically Thin Carbon Films. *Science* **2004,** *306* (5696), 666-669.

108. Gosling, J. H.; Makarovsky, O.; Wang, F.; Cottam, N. D.; Greenaway, M. T.; Patanè, A.; Wildman, R. D.; Tuck, C. J.; Turyanska, L.; Fromhold, T. M., Universal mobility characteristics of graphene originating from charge scattering by ionised impurities. *Communications Physics* **2021,** *4* (1), 30.

109. Morozov, S. V.; Novoselov, K. S.; Katsnelson, M. I.; Schedin, F.; Elias, D. C.; Jaszczak, J. A.; Geim, A. K., Giant Intrinsic Carrier Mobilities in Graphene and Its Bilayer. *Physical Review Letters* **2008,** *100* (1), 016602.
110. Das Sarma, S.; Adam, S.; Hwang, E. H.; Rossi, E., Electronic transport in two-dimensional graphene. *Reviews of Modern Physics* **2011,** *83* (2), 407-470.
111. Hwang, E. H.; Adam, S.; Sarma, S. D., Carrier Transport in Two-Dimensional Graphene Layers. *Physical Review Letters* **2007,** *98* (18), 186806.
112. Bolotin, K. I.; Sikes, K. J.; Jiang, Z.; Klima, M.; Fudenberg, G.; Hone, J.; Kim, P.; Stormer, H. L., Ultrahigh electron mobility in suspended graphene. *Solid State Communications* **2008,** *146* (9), 351-355.
113. Fang, T.; Konar, A.; Xing, H.; Jena, D., Mobility in semiconducting graphene nanoribbons: Phonon, impurity, and edge roughness scattering. *Physical Review B* **2008,** *78* (20), 205403.
114. Liu, Y.; Goolaup, S.; Murapaka, C.; Lew, W. S.; Wong, S. K., Effect of Magnetic Field on the Electronic Transport in Trilayer Graphene. *ACS Nano* **2010,** *4* (12), 7087-7092.
115. Fang, X.-Y.; Yu, X.-X.; Zheng, H.-M.; Jin, H.-B.; Wang, L.; Cao, M.-S., Temperature- and thickness-dependent electrical conductivity of few-layer graphene and graphene nanosheets. *Physics Letters A* **2015,** *379* (37), 2245-2251.
116. Ni, Z. H.; Ponomarenko, L. A.; Nair, R. R.; Yang, R.; Anissimova, S.; Grigorieva, I. V.; Schedin, F.; Blake, P.; Shen, Z. X.; Hill, E. H.; Novoselov, K. S.; Geim, A. K., On Resonant Scatterers As a Factor Limiting Carrier Mobility in Graphene. *Nano Letters* **2010,** *10* (10), 3868-3872.
117. Wang, J.; Zhao, R.; Yang, M.; Liu, Z.; Liu, Z. J. T. J. o. c. p., Inverse relationship between carrier mobility and bandgap in graphene. **2013,** *138 8*, 084701.
118. Scarfe, S.; Cui, W.; Luican-Mayer, A.; Ménard, J.-M., Systematic THz study of the substrate effect in limiting the mobility of graphene. *Scientific Reports* **2021,** *11* (1), 8729.
119. Vitale, V.; Atalar, K.; Mostofi, A. A.; Lischner, J., Flat band properties of twisted transition metal dichalcogenide homo- and heterobilayers of MoS2, MoSe2, WS2 and WSe2. *2D Materials* **2021,** *8* (4), 045010.
120. An, L.; Cai, X.; Pei, D.; Huang, M.; Wu, Z.; Zhou, Z.; Lin, J.; Ying, Z.; Ye, Z.; Feng, X.; Gao, R.; Cacho, C.; Watson, M.; Chen, Y.; Wang, N., Interaction effects and superconductivity signatures in twisted double-bilayer WSe2. *Nanoscale Horizons* **2020,** *5* (9), 1309-1316.
121. Huang, M.; Wu, Z.; Hu, J.; Cai, X.; Li, E.; An, L.; Feng, X.; Ye, Z.; Lin, N.; Law, K. T.; Wang, N., Giant nonlinear Hall effect in twisted bilayer WSe2. *National Science Review* **2023,** *10* (4), nwac232.
122. Lu, J. M.; Zheliuk, O.; Leermakers, I.; Yuan, N. F. Q.; Zeitler, U.; Law, K. T.; Ye, J. T., Evidence for two-dimensional Ising superconductivity in gated MoS2. *Science* **2015,** *350* (6266), 1353-1357.
123. Ramasubramaniam, A.; Naveh, D., Mn-doped monolayer MoS2: An atomically thin dilute magnetic semiconductor. *Physical Review B* **2013,** *87* (19), 195201.
124. Cheng, Y. C.; Zhu, Z. Y.; Mi, W. B.; Guo, Z. B.; Schwingenschlögl, U., Prediction of two-dimensional diluted magnetic semiconductors: Doped monolayer MoS2 systems. *Physical Review B* **2013,** *87* (10), 100401.
125. Peimyoo, N.; Shang, J.; Cong, C.; Shen, X.; Wu, X.; Yeow, E. K. L.; Yu, T., Nonblinking, Intense Two-Dimensional Light Emitter: Monolayer WS2 Triangles. *ACS Nano* **2013,** *7* (12), 10985-10994.
126. Yin, Z.; Li, H.; Li, H.; Jiang, L.; Shi, Y.; Sun, Y.; Lu, G.; Zhang, Q.; Chen, X.; Zhang, H., Single-Layer MoS2 Phototransistors. *ACS Nano* **2012,** *6* (1), 74-80.
127. Larentis, S.; Fallahazad, B.; Tutuc, E., Field-effect transistors and intrinsic mobility in ultra-thin

MoSe2 layers. *Applied Physics Letters* **2012,** *101*.
128. Mak, K. F.; Xiao, D.; Shan, J., Light–valley interactions in 2D semiconductors. *Nature Photonics* **2018,** *12* (8), 451-460.
129. Li, S.; Wang, H.; Wang, J.; Chen, H.; Shao, L., Control of light-valley interactions in 2D transition metal dichalcogenides with nanophotonic structures. *Nanoscale* **2021,** *13 13*, 6357-6372.
130. Somvanshi, D.; Jit, S., 5 - Transition metal dichalcogenides based two-dimensional heterostructures for optoelectronic applications. In *2D Nanoscale Heterostructured Materials*, Jit, S.; Das, S., Eds. Elsevier: 2020; pp 125-149.
131. Sharma, U.; Rana, J. S.; Kumar, C.; Pradeepkumar, M. S.; Ahmad, M. I.; Jit, S.; Das, S., Visible light detection property of seamless two-dimensional MoS2–based metal-semiconductor-metal photodiodes fabricated on silicon substrates. *Materials Science in Semiconductor Processing* **2022,** *151*, 106987.
132. Fan, X.-L.; An, Y.-R.; Guo, W.-J., Ferromagnetism in Transitional Metal-Doped MoS2 Monolayer. *Nanoscale Research Letters* **2016,** *11* (1), 154.
133. Wang, J.; Sun, F.; Yang, S.; Li, Y.; Zhao, C.; Xu, M.; Zhang, Y.; Zeng, H., Robust ferromagnetism in Mn-doped MoS2 nanostructures. *Applied Physics Letters* **2016,** *109*.
134. Zhang, K.; Bersch, B.; Joshi, J.; Addou, R.; Cormier, C.; Zhang, C.; Xu, K.; Briggs, N.; Wang, K.; Subramanian, S.; Cho, K.; Fullerton-Shirey, S.; Wallace, R.; Vora, P.; Robinson, J., Tuning the Electronic and Photonic Properties of Monolayer MoS2 via In Situ Rhenium Substitutional Doping. *Advanced Functional Materials* **2018,** *28*, 1706950.
135. Gao, H.; Suh, J.; Cao, M. C.; Joe, A. Y.; Mujid, F.; Lee, K.-H.; Xie, S.; Poddar, P.; Lee, J.-U.; Kang, K.; Kim, P.; Muller, D. A.; Park, J., Tuning Electrical Conductance of MoS2 Monolayers through Substitutional Doping. *Nano Letters* **2020,** *20* (6), 4095-4101.
136. Kozhakhmetov, A.; Schuler, B.; Tan, A. M. Z.; Cochrane, K. A.; Nasr, J. R.; El-Sherif, H. M.; Bansal, A.; Vera, A.; Bojan, V.; Redwing, J. M.; Bassim, N. D.; Das, S.; Hennig, R. G.; Weber-Bargioni, A.; Robinson, J. A. J. A. M., Scalable Substitutional Re-Doping and its Impact on the Optical and Electronic Properties of Tungsten Diselenide. **2020,** *32*.
137. Tang, L.; Xu, R.; Tan, J.; Yuting, L.; Zou, J.; Zongteng, Z.; Zhang, R.; Zhao, Y.; Lin, J.; Zou, X.; Liu, B.; Cheng, H.-M., *Modulating Electronic Structure of Monolayer Transition Metal Dichalcogenides by Substitutional Nb-Doping*. 2020.
138. Seo, J.; Son, E.; Kim, J.; Kim, S.-W.; Baik, J. M.; Park, H., Controllable substitutional vanadium doping in wafer-scale molybdenum disulfide films. *Nano Research* **2023,** *16* (2), 3415-3421.
139. Zhang, K.; Deng, D.; Zheng, B.; Wang, Y.; Perkins, F. K.; Briggs, N. C.; Crespi, V. H.; Robinson, J. A. J. A. M. I., Tuning Transport and Chemical Sensitivity via Niobium Doping of Synthetic MoS2. *Advanced Materials Interfaces* **2020,** *7*.
140. Zhao, H.; Zhang, G.; Yan, B.; Ning, B.; Wang, C.; Zhao, Y.; Shi, X., Substantially Enhanced Properties of 2D WS2 by High Concentration of Erbium Doping against Tungsten Vacancy Formation. *Research 2022*.
141. Li, W.; Huang, J.; Han, B.; Xie, C.; Huang, X.; Tian, K.; Zeng, Y.; Zhao, Z.; Gao, P.; Zhang, Y.; Yang, T.; Zhang, Z.; Sun, S.; Hou, Y. J. A. S., Molten-Salt-Assisted Chemical Vapor Deposition Process for Substitutional Doping of Monolayer MoS2 and Effectively Altering the Electronic Structure and Phononic Properties. *Advanced Science* **2020,** *7*.
142. Han, X.; Benkraouda, M.; Amrane, N., S Vacancy Engineered Electronic and Optoelectronic Properties of Ni-Doped MoS2 Monolayer: A Hybrid Functional Study. *Journal of Electronic Materials*

2020, *49* (5), 3234-3241.
143. Alharthi, N. H.; Almotairy, S. M.; Alharbi, H. F.; Shahinuzzaman, M.; Luqman, M.; Sobayel, K., Investigation on structural and opto-electronic properties of substitutional Sn doped WS2 by co-sputtering technique. *Journal of Materials Research and Technology* **2021,** *15*, 846-854.
144. Chang, R.-J.; Sheng, Y.; Ryu, G. H.; Mkhize, N.; Chen, T.; Lu, Y.; Chen, J.; Lee, J. K.; Bhaskaran, H.; Warner, J. H., Postgrowth Substitutional Tin Doping of 2D WS2 Crystals Using Chemical Vapor Deposition. *ACS Applied Materials & Interfaces* **2019,** *11* (27), 24279-24288.
145. Kim, Y.; Bark, H.; Kang, B.; Lee, C., Wafer-Scale Substitutional Doping of Monolayer MoS2 Films for High-Performance Optoelectronic Devices. *ACS Applied Materials & Interfaces* **2019,** *11* (13), 12613-12621.
146. Jin, C.; Tao, Z.; Li, T.; Xu, Y.; Tang, Y.; Zhu, J.; Liu, S.; Watanabe, K.; Taniguchi, T.; Hone, J.; Fu, L.; Shan, J.; Mak, K., Stripe phases in WSe2/WS2 moiré superlattices. *Nature Materials* **2021,** *20*, 1-5.
147. Qiu, D. Y.; da Jornada, F. H.; Louie, S. G., Optical Spectrum of MoS2: Many-Body Effects and Diversity of Exciton States. *Physical Review Letters* **2013,** *111* (21), 216805.
148. Regan, E. C.; Wang, D.; Jin, C.; Bakti Utama, M. I.; Gao, B.; Wei, X.; Zhao, S.; Zhao, W.; Zhang, Z.; Yumigeta, K.; Blei, M.; Carlström, J. D.; Watanabe, K.; Taniguchi, T.; Tongay, S.; Crommie, M.; Zettl, A.; Wang, F., Mott and generalized Wigner crystal states in WSe2/WS2 moiré superlattices. *Nature* **2020,** *579* (7799), 359-363.
149. Shimazaki, Y.; Schwartz, I.; Watanabe, K.; Taniguchi, T.; Kroner, M.; Imamoğlu, A., Strongly correlated electrons and hybrid excitons in a moiré heterostructure. *Nature* **2020,** *580* (7804), 472-477.
150. Tang, Y.; Li, L.; Li, T.; Xu, Y.; Liu, S.; Barmak, K.; Watanabe, K.; Taniguchi, T.; MacDonald, A. H.; Shan, J.; Mak, K. F., Simulation of Hubbard model physics in WSe2/WS2 moiré superlattices. *Nature* **2020,** *579* (7799), 353-358.
151. Wang, L.; Shih, E.-M.; Ghiotto, A.; Xian, L.; Rhodes, D. A.; Tan, C.; Claassen, M.; Kennes, D. M.; Bai, Y.; Kim, B.; Watanabe, K.; Taniguchi, T.; Zhu, X.; Hone, J.; Rubio, A.; Pasupathy, A. N.; Dean, C. R., Correlated electronic phases in twisted bilayer transition metal dichalcogenides. *Nature Materials* **2020,** *19* (8), 861-866.
152. Xu, Y.; Liu, S.; Rhodes, D. A.; Watanabe, K.; Taniguchi, T.; Hone, J.; Elser, V.; Mak, K. F.; Shan, J., Correlated insulating states at fractional fillings of moiré superlattices. *Nature* **2020,** *587* (7833), 214-218.
153. Zhu, Q.; Tong, Q.; Sun, H.; Wang, Y.; Yao, W., Coulomb effects on topological band inversion in the moiré of WSe2/BAs heterobilayer. *2D Materials* **2019,** *6* (4), 045037.
154. Zhu, L.; Wang, H.; Yang, L., Moiré potential renormalization and ultra-flat bands induced by quasiparticle-plasmon coupling. *npj Computational Materials* **2023,** *9* (1), 8.
155. Liang, Y.; Yang, L., Carrier Plasmon Induced Nonlinear Band Gap Renormalization in Two-Dimensional Semiconductors. *Physical Review Letters* **2015,** *114* (6), 063001.
156. Wu, C.; Bergman, D.; Balents, L.; Das Sarma, S., Flat Bands and Wigner Crystallization in the Honeycomb Optical Lattice. *Physical Review Letters* **2007,** *99* (7), 070401.
157. Jaworowski, B.; Güçlü, A. D.; Kaczmarkiewicz, P.; Kupczyński, M.; Potasz, P.; Wójs, A., Wigner crystallization in topological flat bands. *New Journal of Physics* **2018,** *20* (6), 063023.
158. Alexeev, E. M.; Ruiz-Tijerina, D. A.; Danovich, M.; Hamer, M. J.; Terry, D. J.; Nayak, P. K.; Ahn, S.; Pak, S.; Lee, J.; Sohn, J. I.; Molas, M. R.; Koperski, M.; Watanabe, K.; Taniguchi, T.; Novoselov, K. S.; Gorbachev, R. V.; Shin, H. S.; Fal'ko, V. I.; Tartakovskii, A. I., Resonantly hybridized

excitons in moiré superlattices in van der Waals heterostructures. *Nature* **2019,** *567* (7746), 81-86.
159. Jin, C.; Regan, E. C.; Yan, A.; Iqbal Bakti Utama, M.; Wang, D.; Zhao, S.; Qin, Y.; Yang, S.; Zheng, Z.; Shi, S.; Watanabe, K.; Taniguchi, T.; Tongay, S.; Zettl, A.; Wang, F., Observation of moiré excitons in WSe2/WS2 heterostructure superlattices. *Nature* **2019,** *567* (7746), 76-80.
160. Seyler, K. L.; Rivera, P.; Yu, H.; Wilson, N. P.; Ray, E. L.; Mandrus, D. G.; Yan, J.; Yao, W.; Xu, X., Signatures of moiré-trapped valley excitons in MoSe2/WSe2 heterobilayers. *Nature* **2019,** *567* (7746), 66-70.
161. Tran, K.; Moody, G.; Wu, F.; Lu, X.; Choi, J.; Kim, K.; Rai, A.; Sanchez, D. A.; Quan, J.; Singh, A.; Embley, J.; Zepeda, A.; Campbell, M.; Autry, T.; Taniguchi, T.; Watanabe, K.; Lu, N.; Banerjee, S. K.; Silverman, K. L.; Kim, S.; Tutuc, E.; Yang, L.; MacDonald, A. H.; Li, X., Evidence for moiré excitons in van der Waals heterostructures. *Nature* **2019,** *567* (7746), 71-75.
162. Liu, E.; Taniguchi, T.; Watanabe, K.; Gabor, N. M.; Cui, Y.-T.; Lui, C. H., Excitonic and Valley-Polarization Signatures of Fractional Correlated Electronic Phases in a WSe2/WS2 Moire Superlattice. *Physical Review Letters* **2021,** *127* (3), 037402.
163. Tong, Q.; Chen, M.; Xiao, F.; Yu, H.; Yao, W., Interferences of electrostatic moiré potentials and bichromatic superlattices of electrons and excitons in transition metal dichalcogenides. *2D Materials* **2021,** *8* (2), 025007.
164. Yu, H.; Yao, W., Luminescence Anomaly of Dipolar Valley Excitons in Homobilayer Semiconductor Moire Superlattices. *Physical Review X* **2021,** *11* (2), 021042.
165. Ge, C.; Zhang, D.; Xiao, F.; Zhao, H.; He, M.; Huang, L.; Hou, S.; Tong, Q.; Pan, A.; Wang, X., Observation and Modulation of High-Temperature Moiré-Locale Excitons in van der Waals Heterobilayers. *ACS Nano* **2023,** *17* (16), 16115-16122.
166. Yuan, L.; Zheng, B.; Kunstmann, J.; Brumme, T.; Kuc, A. B.; Ma, C.; Deng, S.; Blach, D.; Pan, A.; Huang, L., Twist-angle-dependent interlayer exciton diffusion in WS2–WSe2 heterobilayers. *Nature Materials* **2020,** *19* (6), 617-623.
167. Naik, M. H.; Regan, E. C.; Zhang, Z.; Chan, Y.-H.; Li, Z.; Wang, D.; Yoon, Y.; Ong, C. S.; Zhao, W.; Zhao, S.; Utama, M. I. B.; Gao, B.; Wei, X.; Sayyad, M.; Yumigeta, K.; Watanabe, K.; Taniguchi, T.; Tongay, S.; da Jornada, F. H.; Wang, F.; Louie, S. G., Intralayer charge-transfer moiré excitons in van der Waals superlattices. *Nature* **2022,** *609* (7925), 52-57.
168. Andersen, T. I.; Scuri, G.; Sushko, A.; De Greve, K.; Sung, J.; Zhou, Y.; Wild, D. S.; Gelly, R. J.; Heo, H.; Bérubé, D.; Joe, A. Y.; Jauregui, L. A.; Watanabe, K.; Taniguchi, T.; Kim, P.; Park, H.; Lukin, M. D., Excitons in a reconstructed moiré potential in twisted WSe2/WSe2 homobilayers. *Nature Materials* **2021,** *20* (4), 480-487.
169. Wu, F.; Lovorn, T.; Tutuc, E.; Martin, I.; MacDonald, A. H., Topological Insulators in Twisted Transition Metal Dichalcogenide Homobilayers. *Physical Review Letters* **2019,** *122* (8), 086402.
170. Xu, S.-Y.; Ma, Q.; Shen, H.; Fatemi, V.; Wu, S.; Chang, T.-R.; Chang, G.; Valdivia, A. M. M.; Chan, C.-K.; Gibson, Q. D.; Zhou, J.; Liu, Z.; Watanabe, K.; Taniguchi, T.; Lin, H.; Cava, R. J.; Fu, L.; Gedik, N.; Jarillo-Herrero, P., Electrically switchable Berry curvature dipole in the monolayer topological insulator WTe2. *Nature Physics* **2018,** *14* (9), 900-906.
171. Chen, D.; Lian, Z.; Huang, X.; Su, Y.; Rashetnia, M.; Ma, L.; Yan, L.; Blei, M.; Xiang, L.; Taniguchi, T.; Watanabe, K.; Tongay, S.; Smirnov, D.; Wang, Z.; Zhang, C.; Cui, Y.-T.; Shi, S.-F., Excitonic insulator in a heterojunction moiré superlattice. *Nature Physics* **2022,** *18* (10), 1171-1176.
172. Huang, X.; Wang, T.; Miao, S.; Wang, C.; Li, Z.; Lian, Z.; Taniguchi, T.; Watanabe, K.; Okamoto, S.; Xiao, D.; Shi, S.-F.; Cui, Y.-T., Correlated insulating states at fractional fillings of the WS2/WSe2

moiré lattice. *Nature Physics* **2021,** *17* (6), 715-719.
173. Lin, X.; Ni, J., Topologically insulating states in ternary transition metal dichalcogenides. *Journal of Applied Physics* **2017,** *121*, 024303.
174. Li, T.; Jiang, S.; Shen, B.; Zhang, Y.; Li, L.; Tao, Z.; Devakul, T.; Watanabe, K.; Taniguchi, T.; Fu, L.; Shan, J.; Mak, K. F., Quantum anomalous Hall effect from intertwined moiré bands. *Nature* **2021,** *600* (7890), 641-646.
175. Balents, L.; Dean, C. R.; Efetov, D. K.; Young, A. F., Superconductivity and strong correlations in moiré flat bands. *Nature Physics* **2020,** *16* (7), 725-733.
176. Li, T.; Jiang, S.; Li, L.; Zhang, Y.; Kang, K.; Zhu, J.; Watanabe, K.; Taniguchi, T.; Chowdhury, D.; Fu, L.; Shan, J.; Mak, K. F., Continuous Mott transition in semiconductor moiré superlattices. *Nature* **2021,** *597* (7876), 350-354.
177. Li, H.; Kumar, U.; Sun, K.; Lin, S.-Z., Spontaneous fractional Chern insulators in transition metal dichalcogenide moire superlattices. *Physical Review Research* **2021,** *3* (3), L032070.
178. Sheng, D. N.; Gu, Z.-C.; Sun, K.; Sheng, L., Fractional quantum Hall effect in the absence of Landau levels. *Nature Communications* **2011,** *2* (1), 389.
179. Ghiotto, A.; Shih, E.-M.; Pereira, G. S. S. G.; Rhodes, D. A.; Kim, B.; Zang, J.; Millis, A. J.; Watanabe, K.; Taniguchi, T.; Hone, J. C.; Wang, L.; Dean, C. R.; Pasupathy, A. N., Quantum criticality in twisted transition metal dichalcogenides. *Nature* **2021,** *597* (7876), 345-349.
180. Zhou, Y.; Sung, J.; Brutschea, E.; Esterlis, I.; Wang, Y.; Scuri, G.; Gelly, R. J.; Heo, H.; Taniguchi, T.; Watanabe, K.; Zaránd, G.; Lukin, M. D.; Kim, P.; Demler, E.; Park, H., Bilayer Wigner crystals in a transition metal dichalcogenide heterostructure. *Nature* **2021,** *595* (7865), 48-52.
181. Zhang, Y.; Liu, T.; Fu, L., Electronic structures, charge transfer, and charge order in twisted transition metal dichalcogenide bilayers. *Physical Review B* **2021,** *103* (15), 155142.
182. Li, T.; Zhu, J.; Tang, Y.; Watanabe, K.; Taniguchi, T.; Elser, V.; Shan, J.; Mak, K. F., Charge-order-enhanced capacitance in semiconductor moiré superlattices. *Nature Nanotechnology* **2021,** *16* (10), 1068-1072.
183. Cai, J.; Anderson, E.; Wang, C.; Zhang, X.; Liu, X.; Holtzmann, W.; Zhang, Y.; Fan, F.; Taniguchi, T.; Watanabe, K.; Ran, Y.; Cao, T.; Fu, L.; Xiao, D.; Yao, W.; Xu, X., Signatures of Fractional Quantum Anomalous Hall States in Twisted MoTe2. *Nature* **2023**.
184. Anderson, E.; Fan, F.-R.; Cai, J.; Holtzmann, W.; Taniguchi, T.; Watanabe, K.; Xiao, D.; Yao, W.; Xu, X., Programming correlated magnetic states with gate-controlled moiré geometry. *Science* **2023,** *381* (6655), 325-330.
185. Venkateswarlu, S.; Honecker, A.; Trambly de Laissardière, G., Electronic localization in twisted bilayer MoS2 with small rotation angle. *Physical Review B* **2020,** *102* (8), 081103.
186. Devakul, T.; Crépel, V.; Zhang, Y.; Fu, L., Magic in twisted transition metal dichalcogenide bilayers. *Nature Communications* **2021,** *12* (1), 6730.
187. Foutty, B. A.; Kometter, C. R.; Devakul, T.; Reddy, A. P.; Watanabe, K.; Taniguchi, T.; Fu, L.; Feldman, B. E. In *Mapping twist-tuned multi-band topology in bilayer WSe2*, 2023.
188. Rosenberger, M. R.; Chuang, H.-J.; Phillips, M.; Oleshko, V. P.; McCreary, K. M.; Sivaram, S. V.; Hellberg, C. S.; Jonker, B. T., Twist Angle-Dependent Atomic Reconstruction and Moiré Patterns in Transition Metal Dichalcogenide Heterostructures. *ACS Nano* **2020,** *14* (4), 4550-4558.
189. Xu, Y.; Kang, K.; Watanabe, K.; Taniguchi, T.; Mak, K. F.; Shan, J., A tunable bilayer Hubbard model in twisted WSe2. *Nature Nanotechnology* **2022,** *17* (9), 934-939.
190. Rademaker, L., Spin-orbit coupling in transition metal dichalcogenide heterobilayer flat bands.

Physical Review B **2022,** *105* (19), 195428.
191. Lu, X.; Zhou, P.; Chen, S.; Sun, L., Strain-induced two-dimensional topological insulators in monolayer 1T′-RuO2. *Journal of Physics: Condensed Matter* **2022,** *34* (47), 475502.
192. Paul, S.; Talukdar, S.; Singh, R. S.; Saha, S. J. p. s. s. R. R. L., Topological Phase Transition in MoTe2: A Review. *Physica Status Solidi RRL* **2022,** *17*.
193. Dias, A. C.; Qu, F.; Azevedo, D. L.; Fu, J., Band structure of monolayer transition-metal dichalcogenides and topological properties of their nanoribbons: Next-nearest-neighbor hopping. *Physical Review B* **2018,** *98* (7), 075202.
194. Shishidou, T.; Suh, H. G.; Brydon, P. M. R.; Weinert, M.; Agterberg, D. F., Topological band and superconductivity in UTe2. *Physical Review B* **2021,** *103* (10), 104504.
195. Yu, G.; Wen, L.; Luo, G.; Wang, Y., Band structures and topological properties of twisted bilayer MoTe2 and WSe2. *Physica Scripta* **2021,** *96* (12), 125874.
196. Wu, F.; Lovorn, T.; MacDonald, A. H., Topological Exciton Bands in Moire Heterojunctions. *Physical Review Letters* **2017,** *118* (14), 147401.
197. AlBuhairan, H.; Vogl, M. J. a. e.-p. Band structure and band topology in twisted homotrilayer transition metal dichalcogenides 2023, p. arXiv:2306.10881. https://ui.adsabs.harvard.edu/abs/2023arXiv230610881A (accessed June 01, 2023).
198. Huang, A.; Chen, C.-H.; Chang, C.-H.; Jeng, H.-T., Topological Phase and Quantum Anomalous Hall Effect in Ferromagnetic Transition-Metal Dichalcogenides Monolayer 1T−VSe2. *Nanomaterials* **2021,** *11* (8), 1998.
199. Zhang, H.; Huang, J.; Wang, Y.; Liu, R.; Huai, X.; Jiang, J.; Anfuso, C., Atomic force microscopy for two-dimensional materials: A tutorial review. *Optics Communications* **2018,** *406*, 3-17.
200. Zhang, Y.; Chang, T.-R.; Zhou, B.; Cui, Y.-T.; Yan, H.; Liu, Z.; Schmitt, F.; Lee, J.; Moore, R.; Chen, Y.; Lin, H.; Jeng, H.-T.; Mo, S.-K.; Hussain, Z.; Bansil, A.; Shen, Z.-X., Direct observation of the transition from indirect to direct bandgap in atomically thin epitaxial MoSe2. *Nature Nanotechnology* **2014,** *9* (2), 111-115.
201. Shi, X.; Qing, W.; Marhaba, T.; Zhang, W., Atomic force microscopy - Scanning electrochemical microscopy (AFM-SECM) for nanoscale topographical and electrochemical characterization: Principles, applications and perspectives. *Electrochimica Acta* **2020,** *332*, 135472.
202. Chang, Y.-Y.; Han, H. N.; Kim, M., Analyzing the microstructure and related properties of 2D materials by transmission electron microscopy. *Applied Microscopy* **2019,** *49* (1), 10.
203. Kwon, S.; Kim, J. M.; Ma, P. J.; Guan, W.; Nam, S. J. A. P. R., Near-Field Nano-Optical Imaging of van der Waals Materials. *Advanced Physics Research* **2023**.
204. Lee, C.; Jeong, B. G.; Kim, S. H.; Kim, D. H.; Yun, S. J.; Choi, W.; An, S.-J.; Lee, D.; Kim, Y.-M.; Kim, K. K.; Lee, S. M.; Jeong, M. S., Investigating heterogeneous defects in single-crystalline WS2 via tip-enhanced Raman spectroscopy. *npj 2D Materials and Applications* **2022,** *6* (1), 67.
205. Shao, J.; Su, W., Tip-enhanced nanoscopy of two-dimensional transition metal dichalcogenides: progress and perspectives. *Nanoscale* **2022,** *14* (46), 17119-17133.
206. Park, K.-D.; Khatib, O.; Kravtsov, V.; Clark, G.; Xu, X.; Raschke, M. B., Hybrid Tip-Enhanced Nanospectroscopy and Nanoimaging of Monolayer WSe2 with Local Strain Control. *Nano Letters* **2016,** *16* (4), 2621-2627.
207. Fei, L.; Lei, S.; Zhang, W.-B.; Lu, W.; Lin, Z.; Lam, C. H.; Chai, Y.; Wang, Y., Direct TEM observations of growth mechanisms of two-dimensional MoS2 flakes. *Nature Communications* **2016,** *7* (1), 12206.

208. Kondekar, N.; Boebinger, M. G.; Tian, M.; Kirmani, M. H.; McDowell, M. T., The Effect of Nickel on MoS2 Growth Revealed with in Situ Transmission Electron Microscopy. *ACS Nano* **2019,** *13* (6), 7117-7126.
209. Zhang, Y.; Zhang, Z.; Cheng, Y.; Cheng, F.; Wang, L.; Liu, N.; Li, L.; Su, J.; Gao, Y., In situ TEM observation of controlled growth of two-dimensional WS2 with vertically aligned layers and high-temperature stability. *Nano Energy* **2020,** *67*, 104221.
210. Mendes, R. G.; Pang, J.; Bachmatiuk, A.; Ta, H. Q.; Zhao, L.; Gemming, T.; Fu, L.; Liu, Z.; Rümmeli, M. H., Electron-Driven In Situ Transmission Electron Microscopy of 2D Transition Metal Dichalcogenides and Their 2D Heterostructures. *ACS Nano* **2019,** *13* (2), 978-995.
211. Lai, K.; Kundhikanjana, W.; Kelly, M.; Shen, Z., Modeling and characterization of a cantilever-based near-field scanning microwave impedance microscope. *The Review of scientific instruments* **2008,** *79*, 063703.
212. Kim, Y.; Kim, J., Near-field optical imaging and spectroscopy of 2D-TMDs. *Nanophotonics* **2021,** *10* (13), 3397-3415.
213. Berweger, S.; Weber, J. C.; John, J.; Velazquez, J. M.; Pieterick, A.; Sanford, N. A.; Davydov, A. V.; Brunschwig, B.; Lewis, N. S.; Wallis, T. M.; Kabos, P., Microwave Near-Field Imaging of Two-Dimensional Semiconductors. *Nano Letters* **2015,** *15* (2), 1122-1127.
214. Lee, K.; Utama, M. I. B.; Kahn, S.; Samudrala, A.; Leconte, N.; Yang, B.; Wang, S.; Watanabe, K.; Taniguchi, T.; Altoé, M. V. P.; Zhang, G.; Weber-Bargioni, A.; Crommie, M.; Ashby, P. D.; Jung, J.; Wang, F.; Zettl, A., Ultrahigh-resolution scanning microwave impedance microscopy of moiré lattices and superstructures. *Science Advances 6* (50), eabd1919.
215. Della Pia, A.; Costantini, G., Scanning Tunneling Microscopy. In *Encyclopedia of Nanotechnology*, Bhushan, B., Ed. Springer Netherlands: Dordrecht, 2012; pp 2301-2313.
216. Binnig, G.; Rohrer, H.; Gerber, C.; Weibel, E., Surface Studies by Scanning Tunneling Microscopy. *Physical Review Letters* **1982,** *49* (1), 57-61.
217. Shabani, S.; Halbertal, D.; Wu, W.; Chen, M.; Liu, S.; Hone, J.; Yao, W.; Basov, D. N.; Zhu, X.; Pasupathy, A. N., Deep moiré potentials in twisted transition metal dichalcogenide bilayers. *Nature Physics* **2021,** *17* (6), 720-725.
218. Raja, A.; Chaves, A.; Yu, J.; Arefe, G.; Hill, H. M.; Rigosi, A. F.; Berkelbach, T. C.; Nagler, P.; Schüller, C.; Korn, T.; Nuckolls, C.; Hone, J.; Brus, L. E.; Heinz, T. F.; Reichman, D. R.; Chernikov, A., Coulomb engineering of the bandgap and excitons in two-dimensional materials. *Nature Communications* **2017,** *8* (1), 15251.
219. Wang, G.; Chernikov, A.; Glazov, M. M.; Heinz, T. F.; Marie, X.; Amand, T.; Urbaszek, B., Colloquium: Excitons in atomically thin transition metal dichalcogenides. *Reviews of Modern Physics* **2018,** *90* (2), 021001.
220. Ugeda, M. M.; Bradley, A. J.; Shi, S.-F.; da Jornada, F. H.; Zhang, Y.; Qiu, D. Y.; Ruan, W.; Mo, S.-K.; Hussain, Z.; Shen, Z.-X.; Wang, F.; Louie, S. G.; Crommie, M. F., Giant bandgap renormalization and excitonic effects in a monolayer transition metal dichalcogenide semiconductor. *Nature Materials* **2014,** *13* (12), 1091-1095.
221. Zhang, C.; Chuu, C.-P.; Ren, X.; Li, M.-Y.; Li, L.-J.; Jin, C.; Chou, M.-Y.; Shih, C.-K., Interlayer couplings, Moire patterns, and 2D electronic superlattices in MoS2/WSe2 hetero-bilayers. *Science Advanced* **2017,** *3* (1), e1601459.
222. Pan, Y.; Fölsch, S.; Nie, Y.; Waters, D.; Lin, Y.-C.; Jariwala, B.; Zhang, K.; Cho, K.; Robinson, J. A.; Feenstra, R. M., Quantum-Confined Electronic States Arising from the Moiré Pattern of MoS2–

WSe2 Heterobilayers. *Nano Letters* **2018,** *18* (3), 1849-1855.
223. Zhang, Z.; Wang, Y.; Watanabe, K.; Taniguchi, T.; Ueno, K.; Tutuc, E.; LeRoy, B. J., Flat bands in twisted bilayer transition metal dichalcogenides. *Nature Physics* **2020,** *16* (11), 1093-1096.
224. Li, E.; Hu, J.-X.; Feng, X.; Zhou, Z.; An, L.; Law, K. T.; Wang, N.; Lin, N., Lattice reconstruction induced multiple ultra-flat bands in twisted bilayer WSe2. *Nature Communications* **2021,** *12* (1), 5601.
225. Liu, K.-K.; Zhang, W.; Lee, Y.-H.; Lin, Y.-C.; Chang, M.-T.; Su, C.-Y.; Chang, C.-S.; Li, H.; Shi, Y.; Zhang, H.; Lai, C.-S.; Li, L.-J., Growth of Large-Area and Highly Crystalline MoS2 Thin Layers on Insulating Substrates. *Nano Letters* **2012,** *12* (3), 1538-1544.
226. Li, H.; Li, S.; Naik, M. H.; Xie, J.; Li, X.; Wang, J.; Regan, E.; Wang, D.; Zhao, W.; Zhao, S.; Kahn, S.; Yumigeta, K.; Blei, M.; Taniguchi, T.; Watanabe, K.; Tongay, S.; Zettl, A.; Louie, S. G.; Wang, F.; Crommie, M. F., Imaging moiré flat bands in three-dimensional reconstructed WSe2/WS2 superlattices. *Nature Materials* **2021,** *20* (7), 945-950.
227. Li, H.; Li, S.; Naik, M. H.; Xie, J.; Li, X.; Regan, E.; Wang, D.; Zhao, W.; Yumigeta, K.; Blei, M.; Taniguchi, T.; Watanabe, K.; Tongay, S.; Zettl, A.; Louie, S. G.; Crommie, M. F.; Wang, F., Imaging local discharge cascades for correlated electrons in WS2/WSe2 moiré superlattices. *Nature Physics* **2021,** *17* (10), 1114-1119.
228. Deshpande, V.; Bockrath, M., The One-Dimensional Wigner Crystal in Carbon Nanotubes. *Nature Physics* **2007,** *4*.
229. Goldman, V. J.; Santos, M.; Shayegan, M.; Cunningham, J. E., Evidence for two-dimentional quantum Wigner crystal. *Physical Review Letters* **1990,** *65* (17), 2189-2192.
230. Jang, J.; Hunt, B.; Pfeiffer, L.; West, K.; Ashoori, R., Sharp tunnelling resonance from the vibrations of an electronic Wigner crystal. *Nature Physics* **2016,** *13*.
231. Padhi, B.; Chitra, R.; Phillips, P. W., Generalized Wigner crystallization in moire materials. *Physical Review B* **2021,** *103* (12), 125146.
232. Shapir, I.; Hamo, A.; Pecker, S.; Moca, C. P.; Legeza, Ö.; Zarand, G.; Ilani, S., Imaging the electronic Wigner crystal in one dimension. *Science* **2019,** *364* (6443), 870-875.
233. Wigner, E., On the Interaction of Electrons in Metals. *Physical Review* **1934,** *46* (11), 1002-1011.
234. Li, H.; Li, S.; Regan, E. C.; Wang, D.; Zhao, W.; Kahn, S.; Yumigeta, K.; Blei, M.; Taniguchi, T.; Watanabe, K.; Tongay, S.; Zettl, A.; Crommie, M. F.; Wang, F., Imaging two-dimensional generalized Wigner crystals. *Nature* **2021,** *597* (7878), 650-654.
235. Li, H.; Xiang, Z.; Naik, M. H.; Kim, W.; Li, Z.; Sailus, R.; Banerjee, R.; Taniguchi, T.; Watanabe, K.; Tongay, S.; Zettl, A.; da Jornada, F. H.; Louie1, S. G.; Crommie, M. F.; Wang, F. J. a. e.-p. Imaging Moiré Excited States with Photocurrent Tunneling Microscopy 2023, p. arXiv:2306.00859. https://ui.adsabs.harvard.edu/abs/2023arXiv230600859L (accessed June 01, 2023).
236. Li, T.; Jiang, S.; Li, L.; Zhang, Y.; Kang, K.; Zhu, J.; Watanabe, K.; Taniguchi, T.; Chowdhury, D.; Fu, L.; Shan, J.; Mak, K., Continuous Mott transition in semiconductor moiré superlattices. *Nature* **2021,** *597*, 350-354.
237. Morales-Durán, N.; MacDonald, A. H.; Potasz, P., Metal-insulator transition in transition metal dichalcogenide heterobilayer moire superlattices. *Physical Review B* **2021,** *103* (24), L241110.
238. Pan, H.; Das Sarma, S., Interaction-Driven Filling-Induced Metal-Insulator Transitions in 2D Moire Lattices. *Physical Review Letters* **2021,** *127* (9), 096802.
239. Zhang, Y.-H., Doping a Mott insulator with excitons in a moire bilayer: Fractional superfluid, neutral Fermi surface, and Mott transition. *Physical Review B* **2022,** *106* (19), 195120.
240. Gu, J.; Ma, L.; Liu, S.; Watanabe, K.; Taniguchi, T.; Hone, J.; Shan, J.; Mak, K., Dipolar excitonic

insulator in a moiré lattice. *Nature Physics* **2022,** *18*, 1-6.
241. Ma, L.; Nguyen, P.; Wang, Z.; Zeng, Y.; Watanabe, K.; Taniguchi, T.; MacDonald, A.; Mak, K.; Shan, J., Strongly correlated excitonic insulator in atomic double layers. *Nature* **2021,** *598*, 585-589.
242. Xu, Y.; Liu, S.; Rhodes, D. A.; Watanabe, K.; Taniguchi, T.; Hone, J. C.; Elser, V.; Mak, K. F.; Shan, J. J. a. S. C. E., Abundance of correlated insulating states at fractional fillings of WSe2/WS2 moire superlattices. **2020**.
243. Park, H.; Zhu, J.; Wang, X.; Wang, Y.; Holtzmann, W.; Taniguchi, T.; Watanabe, K.; Yan, J.; Fu, L.; Cao, T.; Xiao, D.; Gamelin, D. R.; Yu, H.; Yao, W.; Xu, X., Dipole ladders with large Hubbard interaction in a moiré exciton lattice. *Nature Physics* **2023,** *19* (9), 1286-1292.
244. Xiong, R.; Nie, J. H.; Brantly, S. L.; Hays, P.; Sailus, R.; Watanabe, K.; Taniguchi, T.; Tongay, S.; Jin, C., Correlated insulator of excitons in WSe2/WS2 moiré superlattices. *Science* **2023,** *380* (6647), 860-864.
245. Tang, Y.; Gu, J.; Liu, S.; Watanabe, K.; Taniguchi, T.; Hone, J. C.; Mak, K. F.; Shan, J., Dielectric catastrophe at the Wigner-Mott transition in a moiré superlattice. *Nature Communications* **2022,** *13* (1), 4271.
246. Wu, C.-L.; Yuan, H.; Li, Y.; Gong, Y.; Hwang, H. Y.; Cui, Y., Gate-Induced Metal–Insulator Transition in MoS2 by Solid Superionic Conductor LaF3. *Nano Letters* **2018,** *18* (4), 2387-2392.
247. Slagle, K.; Fu, L., Charge transfer excitations, pair density waves, and superconductivity in moir\'e materials. *Physical Review B* **2020,** *102* (23), 235423.
248. Hsu, Y.-T.; Vaezi, A.; Fischer, M. H.; Kim, E.-A., Topological superconductivity in monolayer transition metal dichalcogenides. *Nature Communications* **2017,** *8* (1), 14985.
249. Shi, W.; Ye, J.; Zhang, Y.; Suzuki, R.; Yoshida, M.; Miyazaki, J.; Inoue, N.; Saito, Y.; Iwasa, Y., Superconductivity Series in Transition Metal Dichalcogenides by Ionic Gating. *Scientific Reports* **2015,** *5* (1), 12534.
250. Costanzo, D.; Zhang, H.; Reddy, B. A.; Berger, H.; Morpurgo, A. F., Tunnelling spectroscopy of gate-induced superconductivity in MoS2. *Nature Nanotechnology* **2018,** *13* (6), 483-488.
251. Shimazu, Y.; Yamada, K.; Kobayashi, H.; Ishikawa, R.; Watanabe, H.; Shinchi, T.; Yanai, K., Tunneling spectroscopy of field-induced superconductivity in molybdenum disulfide using top metal contacts. *AIP Advances* **2023**.
252. Costanzo, D.; Jo, S.; Berger, H.; Morpurgo, A. F., Gate-induced superconductivity in atomically thin MoS2 crystals. *Nature Nanotechnology* **2016,** *11* (4), 339-344.
253. Saito, Y.; Nakamura, Y.; Bahramy, M. S.; Kohama, Y.; Ye, J.; Kasahara, Y.; Nakagawa, Y.; Onga, M.; Tokunaga, M.; Nojima, T.; Yanase, Y.; Iwasa, Y., Superconductivity protected by spin–valley locking in ion-gated MoS2. *Nature Physics* **2016,** *12* (2), 144-149.
254. Dvir, T.; Massee, F.; Attias, L.; Khodas, M.; Aprili, M.; Quay, C. H. L.; Steinberg, H., Spectroscopy of bulk and few-layer superconducting NbSe2 with van der Waals tunnel junctions. *Nature Communications* **2018,** *9* (1), 598.
255. Zhang, Y.; Yuan, N. F. Q.; Fu, L., Moire quantum chemistry: Charge transfer in transition metal dichalcogenide superlattices. *Physical Review B* **2020,** *102* (20), 201115.
256. Xu, X.; Yao, W.; Xiao, D.; Heinz, T. F., Spin and pseudospins in layered transition metal dichalcogenides. *Nature Physics* **2014,** *10*, 343 - 350.
257. Yu, Y.; Zhang, K.; Parks, H.; Babar, M.; Carr, S.; Craig, I. M.; Van Winkle, M.; Lyssenko, A.; Taniguchi, T.; Watanabe, K.; Viswanathan, V.; Bediako, D. K., Tunable angle-dependent electrochemistry at twisted bilayer graphene with moiré flat bands. *Nature Chemistry* **2022,** *14* (3), 267-

273.
258. Hsieh, V.; Halbertal, D.; Finney, N. R.; Zhu, Z.; Gerber, E.; Pizzochero, M.; Kucukbenli, E.; Schleder, G. R.; Angeli, M.; Watanabe, K.; Taniguchi, T.; Kim, E.-A.; Kaxiras, E.; Hone, J.; Dean, C. R.; Basov, D. N., Domain-Dependent Surface Adhesion in Twisted Few-Layer Graphene: Platform for Moiré-Assisted Chemistry. *Nano Letters* **2023,** *23* (8), 3137-3143.
259. Jiang, Z.; Zhou, W.; Hong, A.; Guo, M.; Luo, X.; Yuan, C., MoS2 Moiré Superlattice for Hydrogen Evolution Reaction. *ACS Energy Letters* **2019,** *4* (12), 2830-2835.
260. Xie, L.; Wang, L.; Zhao, W.; Liu, S.; Huang, W.; Zhao, Q., WS2 moiré superlattices derived from mechanical flexibility for hydrogen evolution reaction. *Nature Communications* **2021,** *12* (1), 5070.